Supporting Information

A photocaged, pH-sensitive anion transporter with AND logic dual-stimuli activation

Bartłomiej Zawada and Michał J. Chmielewski

Contents

1. General information

1.1. Abbreviations

DMSO: dimethyl sulfoxide;

LUV: large unilamellar vesicle;

POPC: 1-palmitoyl-2-oleoylphosphatidylcholine;

SPQ: 6-methoxy-*N*-(3-sulfopropyl)quinolinium.

1.2. Materials

All reagents were purchased from Ambeed, Sigma-Aldrich, or TCI and used without further purification. Deuterated solvents were purchased from Eurisotop. TLC was carried out on Merck Silica Gel 60 F_{254} plates. Preparative chromatography was done using Merck Silica Gel 60 (230-400 mesh). Water was taken from Milli-Q purification system. Sephadex G-50 superfine form GE Healthcare was used for size-exclusion chromatography.

1.3. Instruments and methods

NMR spectra were recorded using Bruker Avance 300 MHz, Agilent 400 MHz or Bruker Avance 500 MHz spectrometers at ambient temperature (unless stated otherwise), in DMSO-d_6. 2D NMR spectra were recorded using Bruker Avance 500 MHz. Chemical shifts are reported in parts per million (ppm) and coupling constants *J* are given in hertz (Hz). Data are reported as follows: chemical shift, multiplicity (s – singlet, d – doublet, t – triplet, m – multiplet), coupling constant, and integration. The residual signal of DMSO solvent was used as an internal reference standard (δH = 2.500 ppm and δC = 39.50 ppm). The HR-ESI mass spectra were obtained using a Shimadzu TOF mass spectrometer with methanol as a spray solvent. For weighing analytical samples, Mettler Toledo Excellence XA105DU analytical balance (readability 0.01 mg) was used. UV-vis spectra were obtained on Thermo Scientific Evolution 300 UV-vis spectrometer. The UV-vis spectra were measured in septum-sealed screw-capped precision cells made of SUPRASIL quartz (optical path length: 10 mm). Fluorescence spectra were acquired using Hitachi F-7000 spectrophotometer equipped with a Peltier temperature controller and septum-sealed screw-capped SUPRASIL quartz fluorescence cuvettes (10 × 10 mm). IKA VORTEX 4 basic, model V4 B S000, was used for vortexing during LUVs preparation. pH measurements were carried out using SevenExcellence pH/cond meter S470 equipped with InLab Expert Pro pH electrode. Photocleavage reactions were carried out in a custom-made photoreactor equipped with 8 × 9 W UV-bulbs (Philips PL-S 9W/2P BLB, $\lambda_{max} \approx 365$ nm, *ca.* 20 nm band width) and a ventilator for cooling (Figure S1). The lamps were switched on and left for 45 minutes to warm up before inserting the samples inside. The UV irradiance in the reactor was found to be *ca.* 490 mW × m^{-2}.[1] AVESTIN LiposoFast-Basic extruder with polycarbonate membranes (pore sizes of 200 nm) was used for extrusion during LUVs preparation.

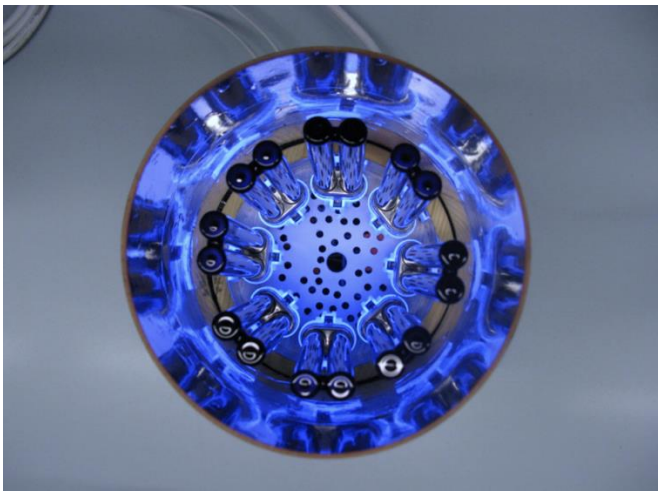

Figure S1. The custom-made photoreactor (top view) used in this study.

2. Synthetic procedures and characterization of new compounds

Synthesis of 1,8-diamino-3,6-dinitrocarbazole 4

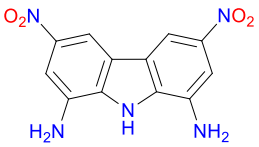

4

$C_{12}H_9N_5O_4$
287.231 g/mol

1,8-Diamino-3,6-dinitrocarbazole **4** was obtained according to the previously published procedure.[2]

Synthesis of bis(ONB)protected 1,8-diamino-3,6-dinitrocarbazole 3

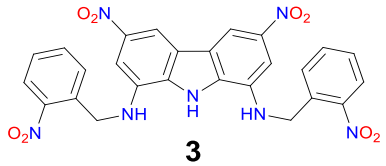

3

$C_{26}H_{19}N_7O_8$
557.471 g/mol

To a 250 ml two-neck round-bottom flask equipped with a magnetic stirrer, **4** (574 mg, 2 mmol), *o*-nitrobenzaldehyde (907 mg, 6 mmol) and *o*-chlorobenzoic acid (138 mg, 0.88 mmol, 44 mol%) were added. Side neck was fitted with a right-angle tubing adapter and connected to an argon inlet. The flask was flushed with argon and, in a counter stream of argon, dry THF (from SPS, 115 ml) was added. Still in a counter stream of argon the main neck was equipped with a reflux condenser connected to a check-valve bubbler. Argon was purged through the apparatus for the additional 5 minutes. After this time, the argon inlet was removed and the reaction was heated to reflux. Upon heating, all solids dissolved and the resulting dark brown solution was stirred under reflux for 20 hours. After this time, a dark yellow precipitate formed, and the reaction mixture was cooled down to room temperature. $NaBH_4$ (227 mg, 6 mmol) was added in three equal batches at 5 minute intervals. After 30 minutes, all of the solid dissolved, resulting in dark brown solution. The reaction mixture was transferred to a 500 ml round-bottom flask, which was closed with a rubber septum and kept under argon atmosphere. In a separate 250 ml two-neck round-bottom flask equipped with a reflux condenser and a check-valve bubbler, Mili-Q water (150 ml) was refluxed under argon. The heating was turned off and, after the water stopped boiling, it was transferred to the reaction mixture *via* a cannula. Upon addition of water some brown precipitate formed, resulting in cloudy mixture. The obtained mixture had a pH of around 9 (measured with a pH-indicator paper) and HCl (2 M in water, 3 ml) was added, resulting in a pH of around 3. After cooling down to room temperature, the mixture was put in a fridge for another 2 hours. After this time, the solid precipitate was filtered off, washed with water (3×20 ml) and dried *in vacuo* to give semi-purified brown product as co-crystal with THF (1:1) (561 mg, 0.89 mmol, 45%).

^{1}H NMR (500 MHz, DMSO-d_6) δ 11.96 (s, 1H), 8.74 (s, 2H), 8.13 (d, *J* = 7.1 Hz, 2H), 7.75 (s, 4H), 7.59 (s, 2H), 7.34 (s, 2H), 6.50 (s, 2H), 4.93 (s, 4H) (Figure S2).

^{13}C NMR (126 MHz, DMSO-d_6) δ 148.4, 142.5, 134.6, 133.9, 133.7, 133.0, 130.0, 128.8, 125.1, 122.4, 108.0, 100.3, 44.1 (Figure S3).

HR MS (ESI): m/z calc. for $C_{26}H_{18}N_7O_8$ $[M–H]^-$: 556.1222; found: 556.1232.

Synthesis of bis(ONB)protected) 1,8-diamidocarbazole 2

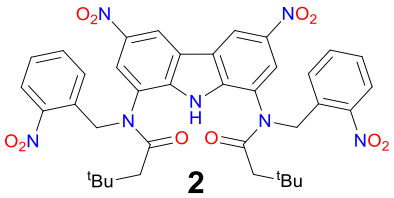

2

$C_{38}H_{39}N_7O_{10}$
753.757 g/mol

A 100 ml single-neck round-bottom flask was dried in a stream of hot air and then cooled down *in vacuo*. Next, it was equipped with a magnetic stir bar and charged with **3** (279 mg, 0.5 mmol). The flask was closed with rubber septum and purged with argon. Acetonitrile (55 ml) was added in the counter stream of argon, forming a dark suspension. Then, pyridine (0.16 ml, 2 mmol) was added dropwise, followed by 3,3-dimethylbutyryl chloride (0.28 ml, 2 mmol). After 24 hours, the reaction mixture was concentrated on rotary evaporator to *ca.* 5 ml and dissolved in 15 ml of ethyl acetate. The mixture was washed with water (3×100 ml) and brine (2×5 ml). Next, the organic layer was dried over $MgSO_4$ and filtered. Next, silica gel (1.8 g) was added, and the volatiles were evaporated on a rotary evaporator. The mixture was separated by column chromatography (DCM/AcOEt 100:0 – 95:5 v/v). Fractions containing pure product were combined and evaporated to yield orange solid (53 mg, 0.07 mmol, 14%).

^{1}H NMR (500 MHz, DMSO-d_6) δ 12.81 (overlapped, 2H); 9.57 (overlapped, 4H); 7.97 (d, J = 1.4 Hz, 2H); 7.92 (overlapped, 4H); 7.87 (d, J = 8.1 Hz, 2H); 7.78 (d, J = 4.1 Hz, 2H); 7.74 (overlapped, 6H); 7.53 (overlapped, 4H); 5.92 (overlapped, 4H); 4.77 (d, J = 16.0 Hz, 2H); 4.63 (d, J = 16.0 Hz, 2H); 2.20 (d, J = 15.3 Hz, 2H); 2.14 (d, J = 15.3 Hz, 2H); 2.04 (d, J = 15.3 Hz, 2H); 1.92 (d, J = 15.3 Hz, 2H); 0.95 (s, 18H); 0.89 (s, 18H) (Figure S4).

^{13}C NMR (126 MHz, DMSO-d_6) δ 171.2, 170.9, 148.9, 141.5, 141.3, 141.3, 133.6, 133.5, 131.6, 131.5, 130.7, 130.4, 128.9, 128.8, 126.3, 126.3, 124.8, 124.7, 124.5, 124.4, 123.3, 123.2, 118.7, 47.7, 47.2, 44.9, 44.7, 30.9, 30.8, 29.6 (Figure S8).

HR MS (ESI): m/z calc. for $C_{38}H_{38}N_7O_{10}$ $[M–H]^-$: 752.2686; found: 752.3148.

Synthesis of 1

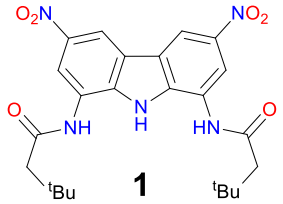

1

$C_{24}H_{29}N_5O_6$
483.517 g/mol

1 was prepared according to the previously published procedure.[2]

3. NMR spectra and proton assignment

3.1. NMR spectra

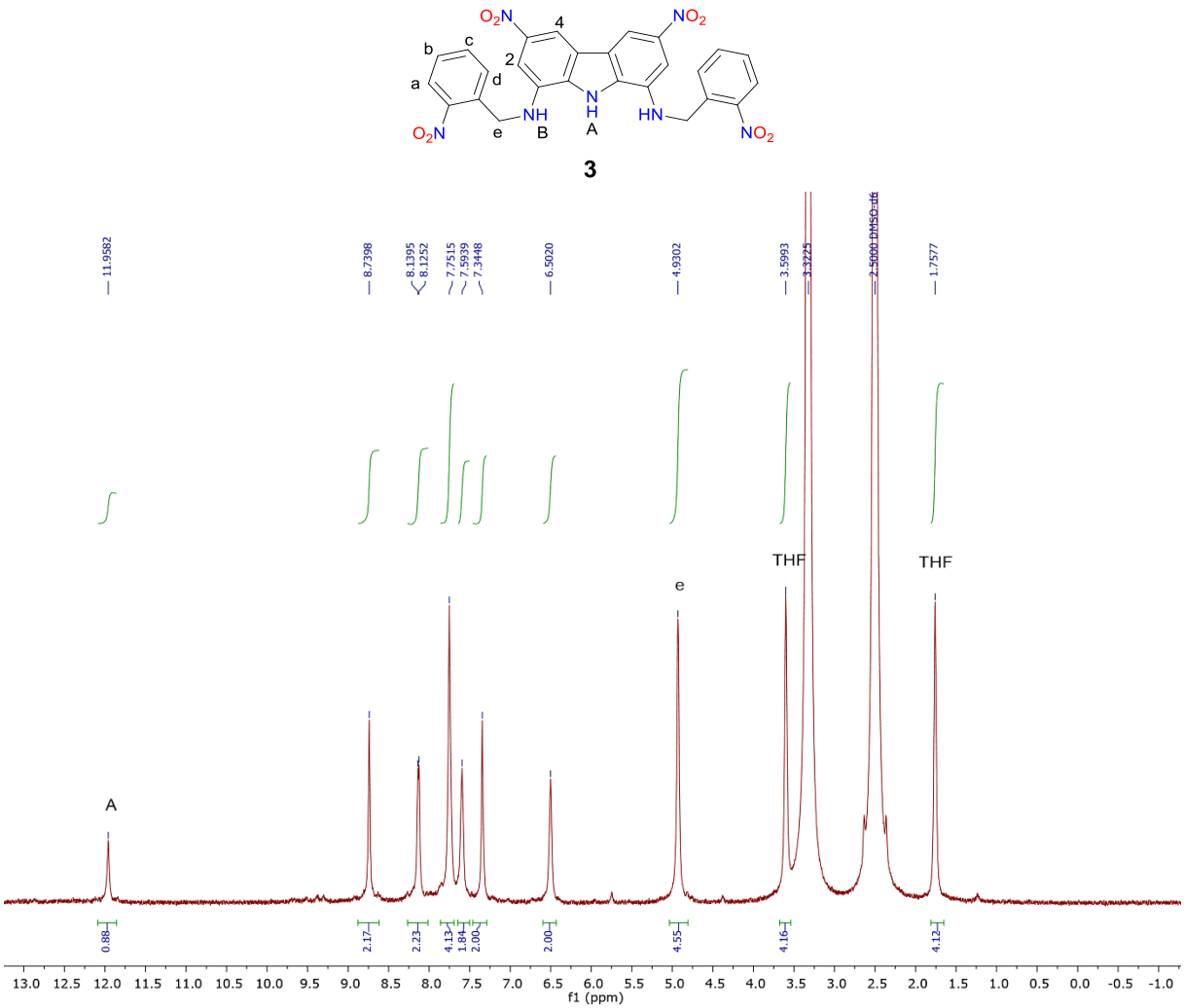

Figure S2. ^{1}H NMR spectrum of **3** in DMSO-d_6. Visible signals from THF in *ca.* 1:1 molar ratio. Recorded using Bruker Avance 500 MHz.

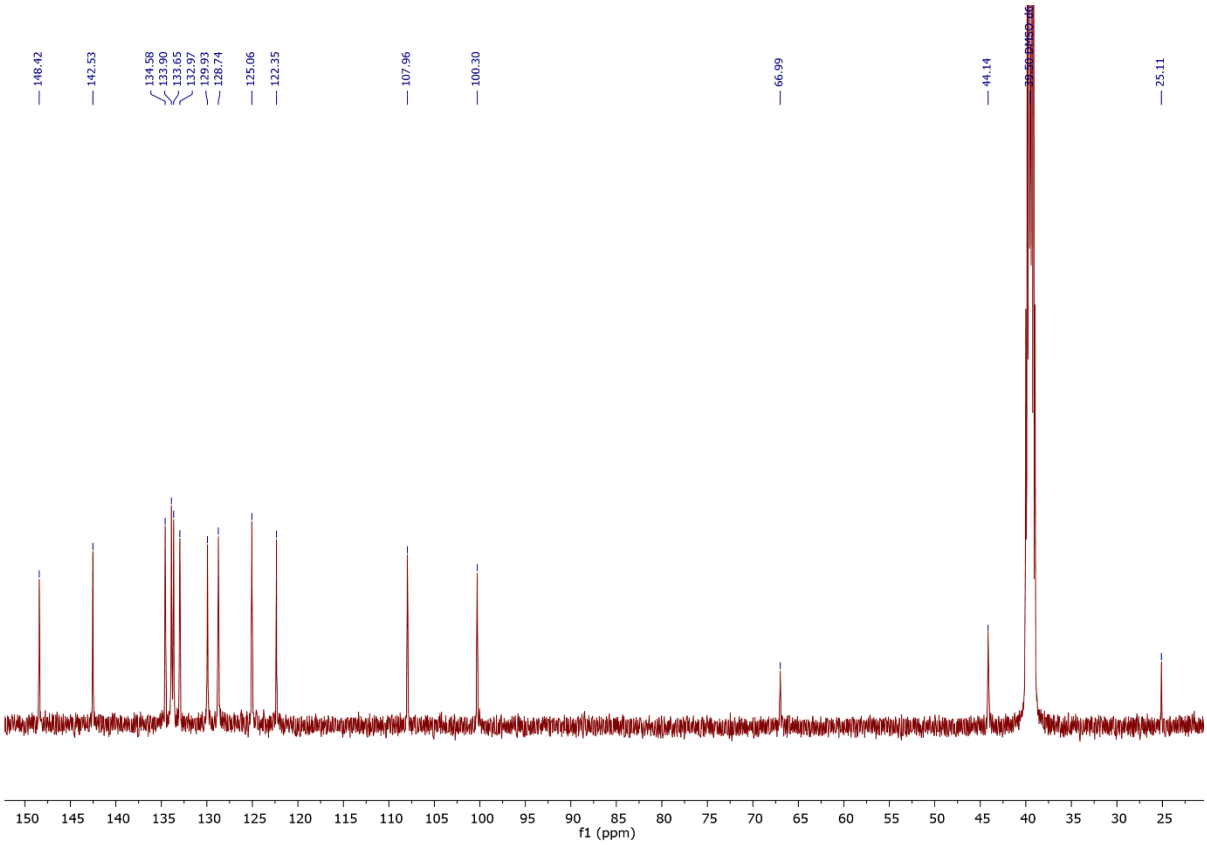

Figure S3. ^{13}C NMR spectrum of **3** in DMSO-d_6. Visible signals from THF. Recorded using Bruker Avance 500 MHz.

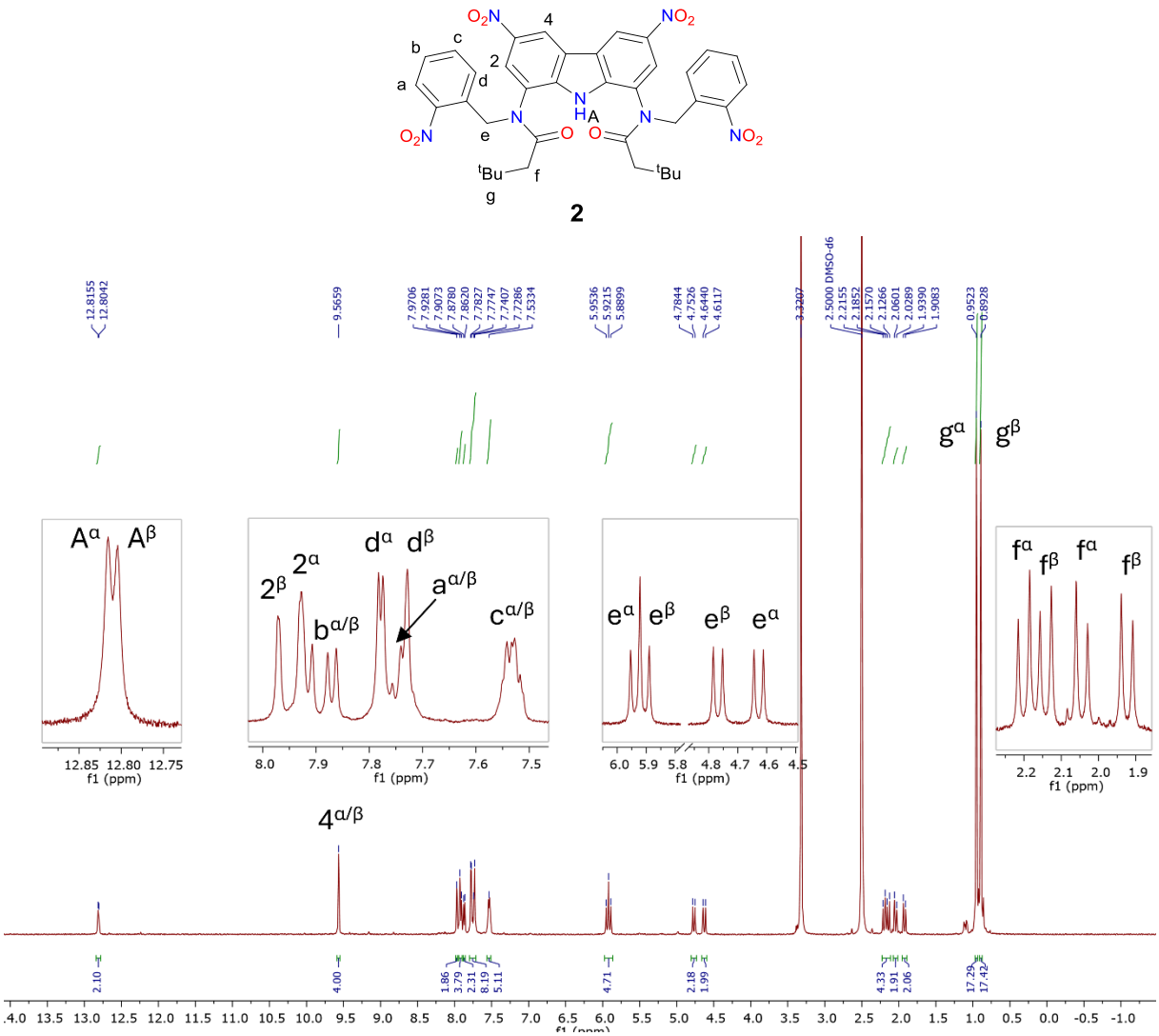

Figure S4. ^{1}H NMR spectrum of **2** in DMSO-d6. Recorded using Bruker Avance 500 MHz.

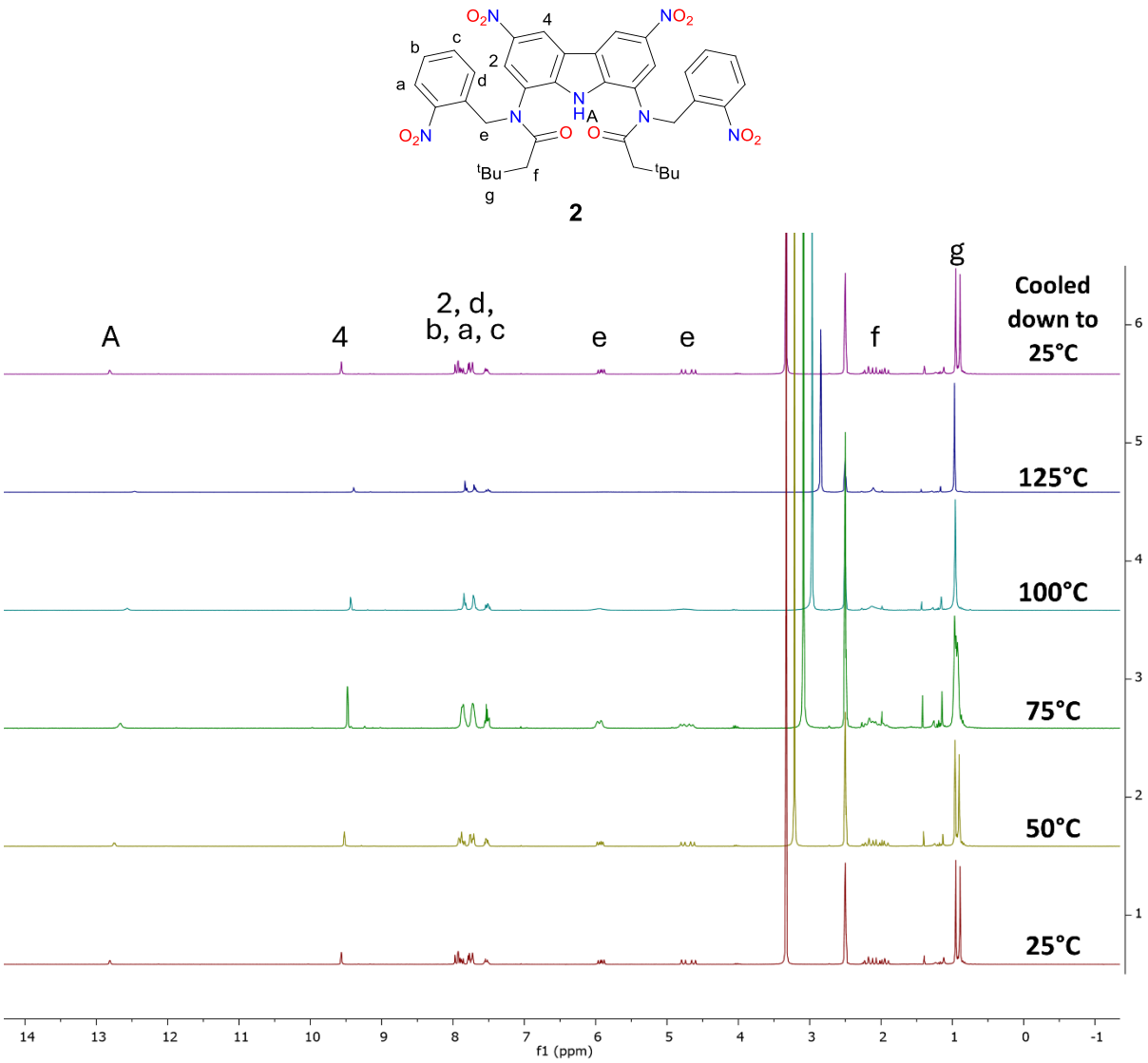

Figure S5. ^{1}H NMR spectra of **2** in DMSO-d_6 in various temperatures. Recorded using Bruker Avance 300 MHz.

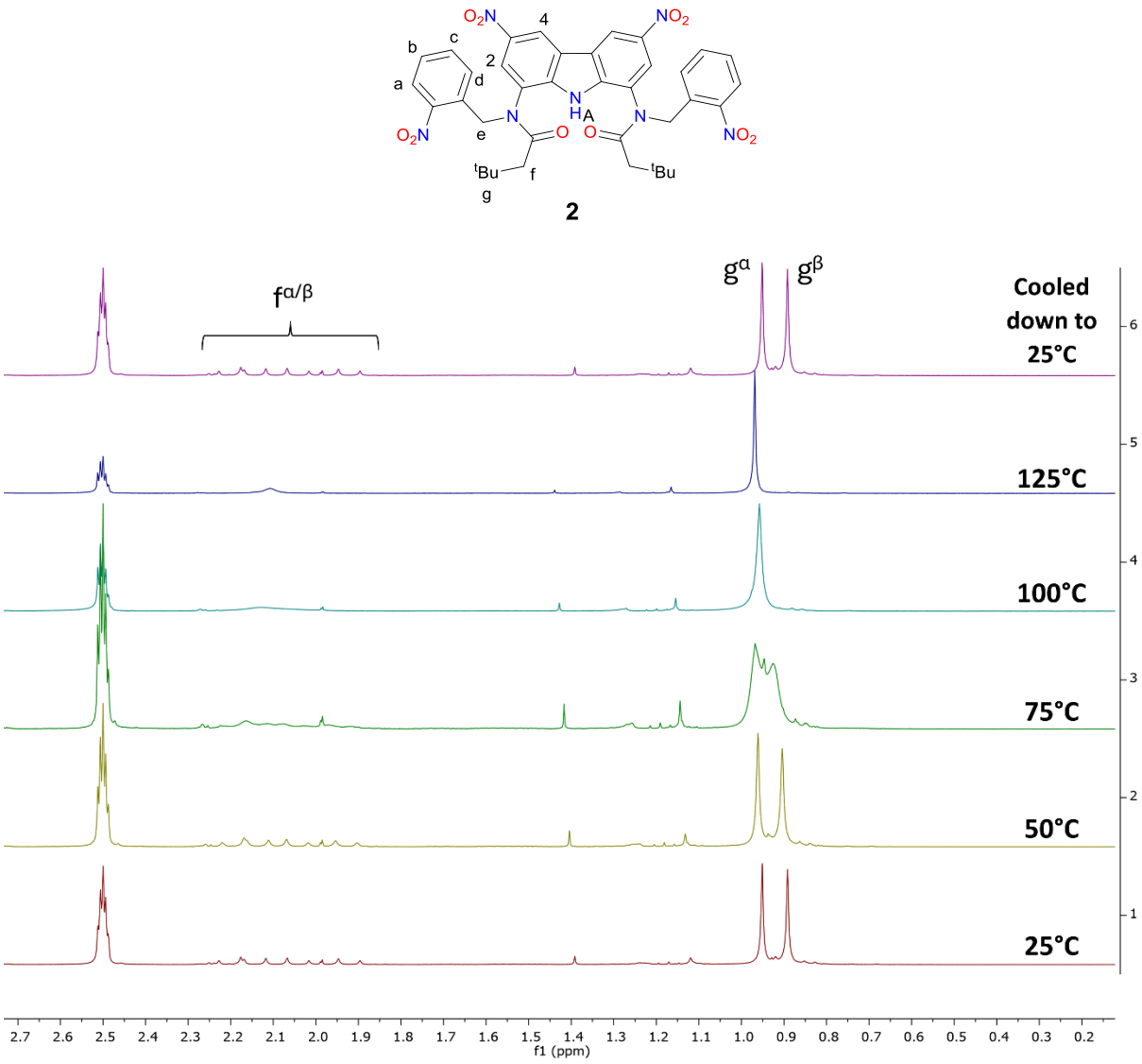

Figure S6. Section of ^{1}H NMR spectra of **2** in DMSO-d_6 in various temperatures. Recorded using Bruker Avance 300 MHz.

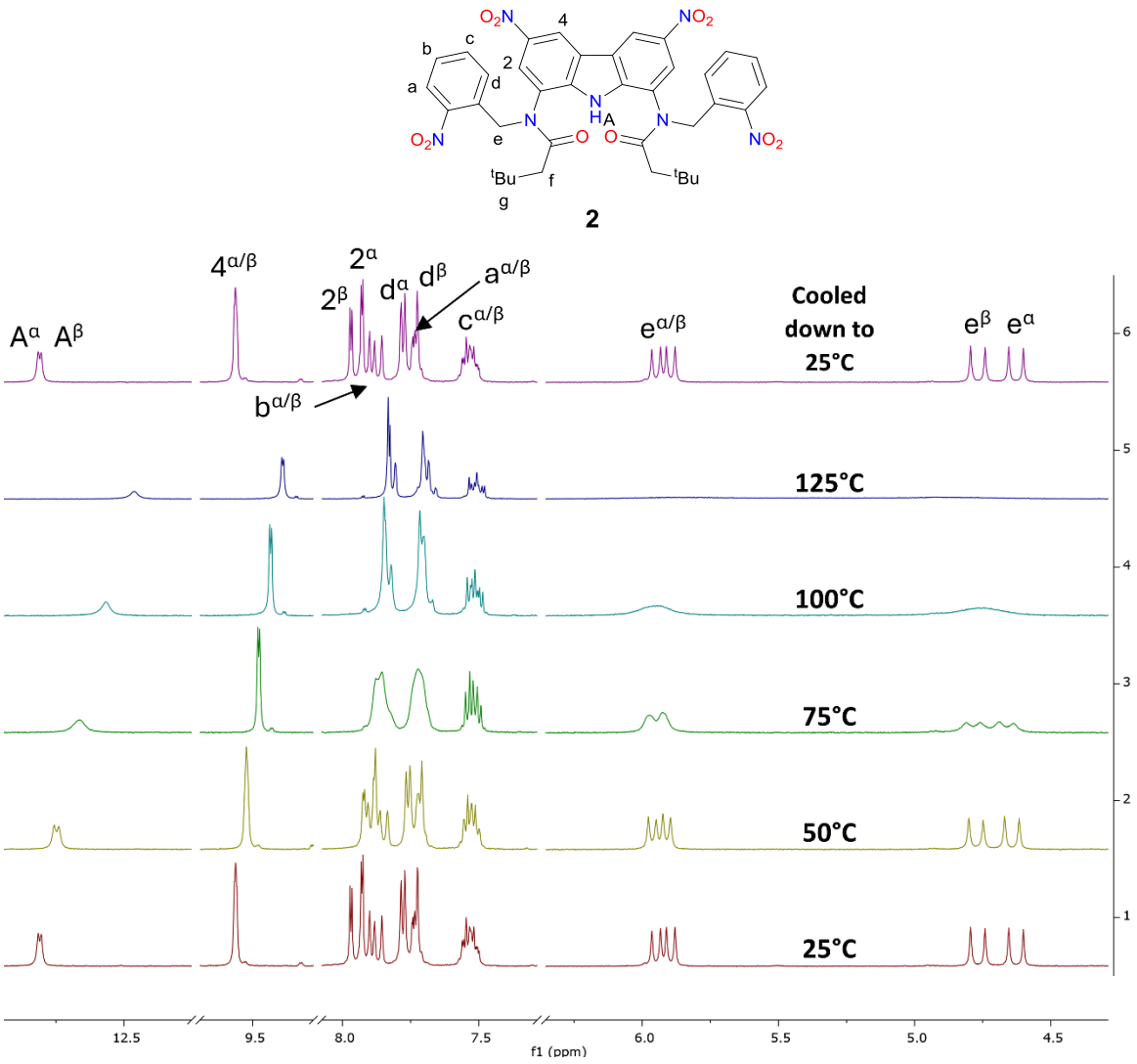

Figure S7. Section of ^{1}H NMR spectra of **2** in DMSO-d_6 in various temperatures. Recorded using Bruker Avance 300 MHz.

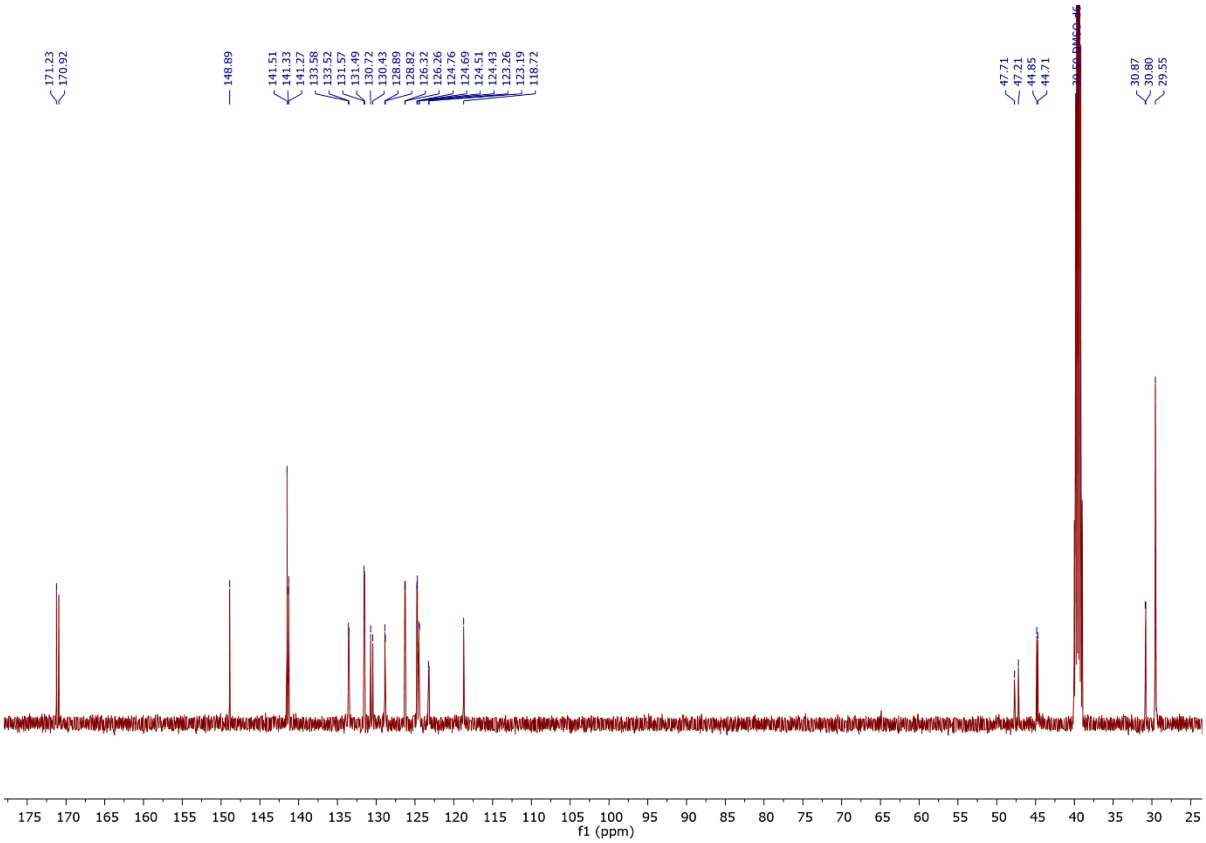

Figure S8. ^{13}C NMR spectrum of **2** in DMSO-d_6. Recorded using Bruker Avance 500 MHz.

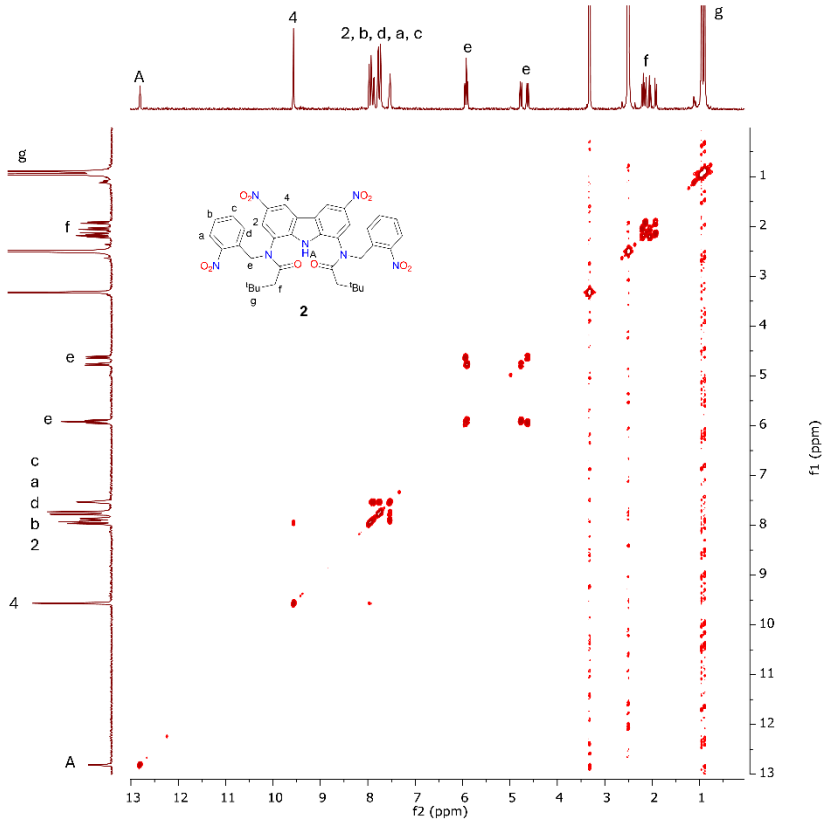

Figure S9. 2D ^{1}H-^{1}H COSY spectrum of **2** in DMSO-d_6.

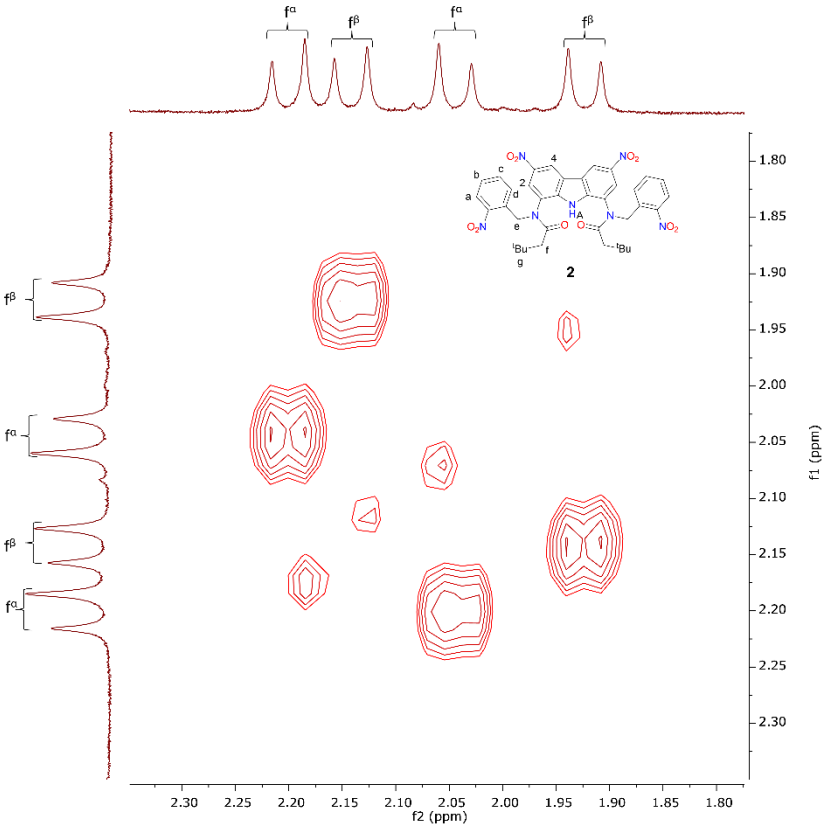

Figure S10. Section of 2D ^{1}H-^{1}H COSY spectrum of **2** in DMSO-d_6.

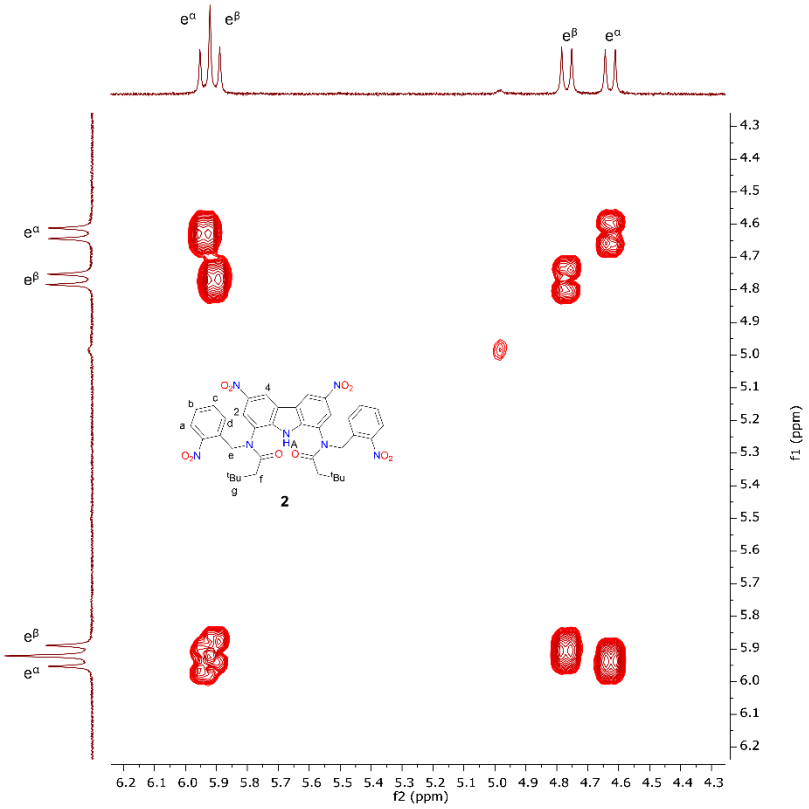

Figure S11. Section of 2D ^{1}H-^{1}H COSY spectrum of **2** in DMSO-d_6.

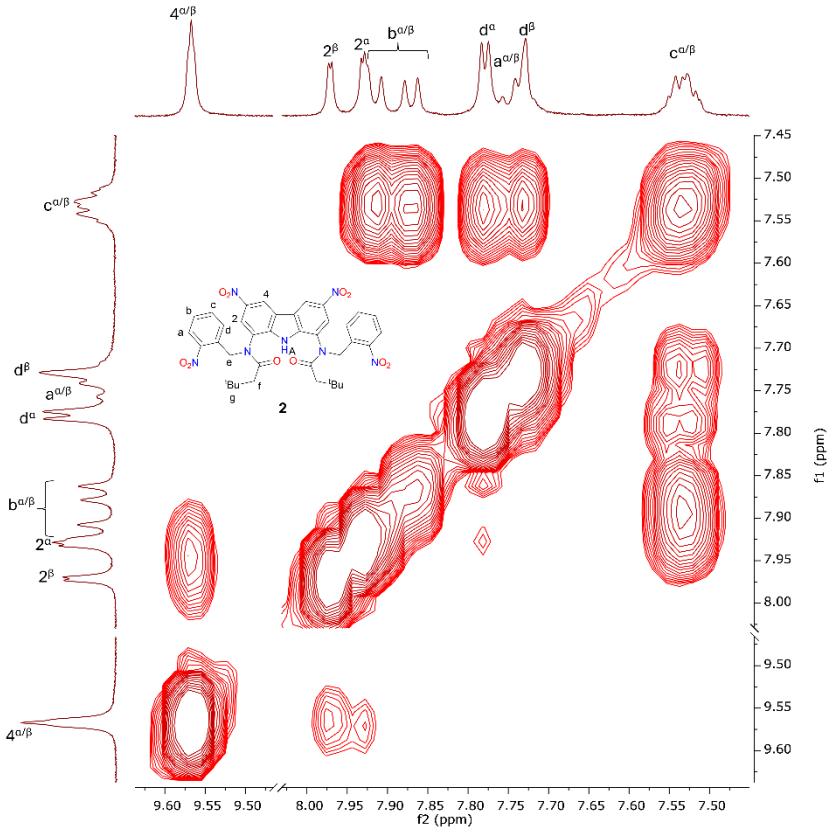

Figure S12. Section of 2D ^{1}H-^{1}H COSY spectrum of **2** in DMSO-d_6.

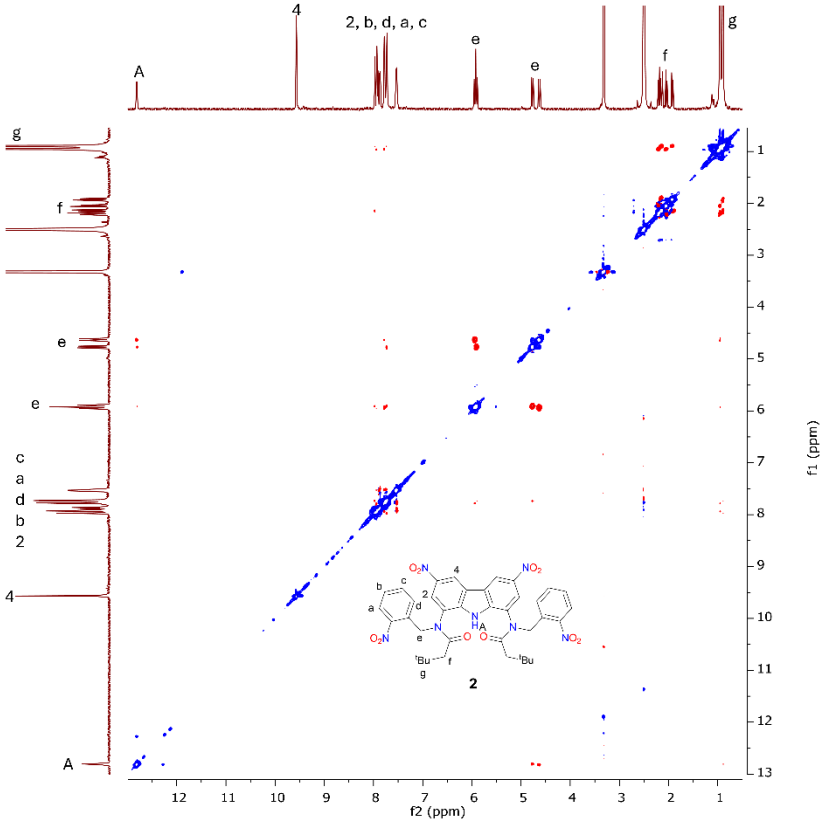

Figure S13. 2D ^{1}H-^{1}H ROESY spectrum of **2** in DMSO-d_6.

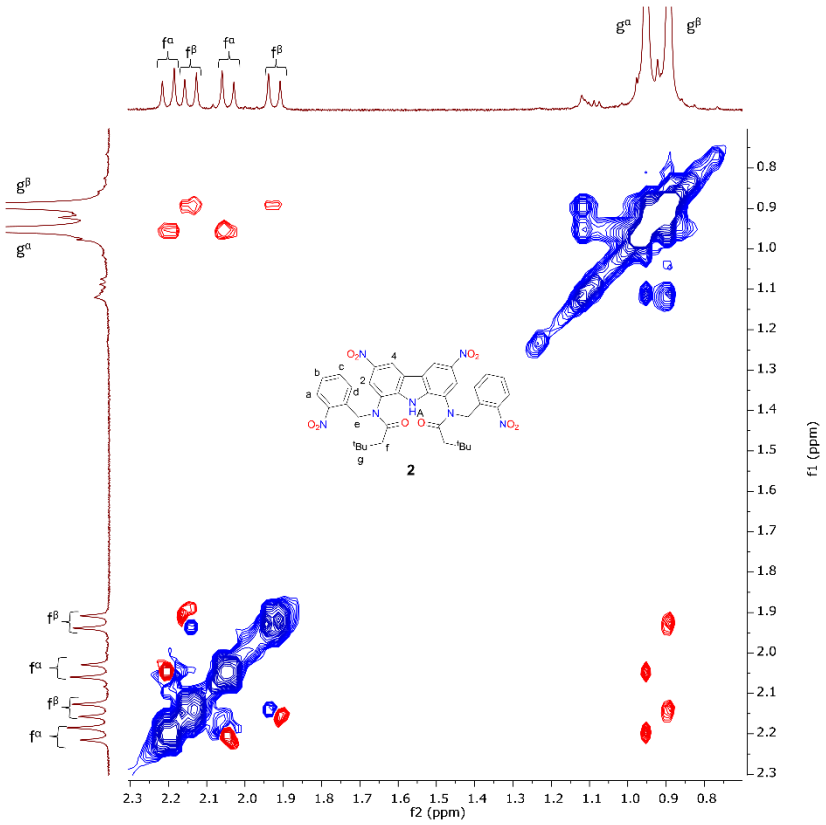

Figure S14. Section of 2D ^{1}H-^{1}H ROESY spectrum of **2** in DMSO-d_6.

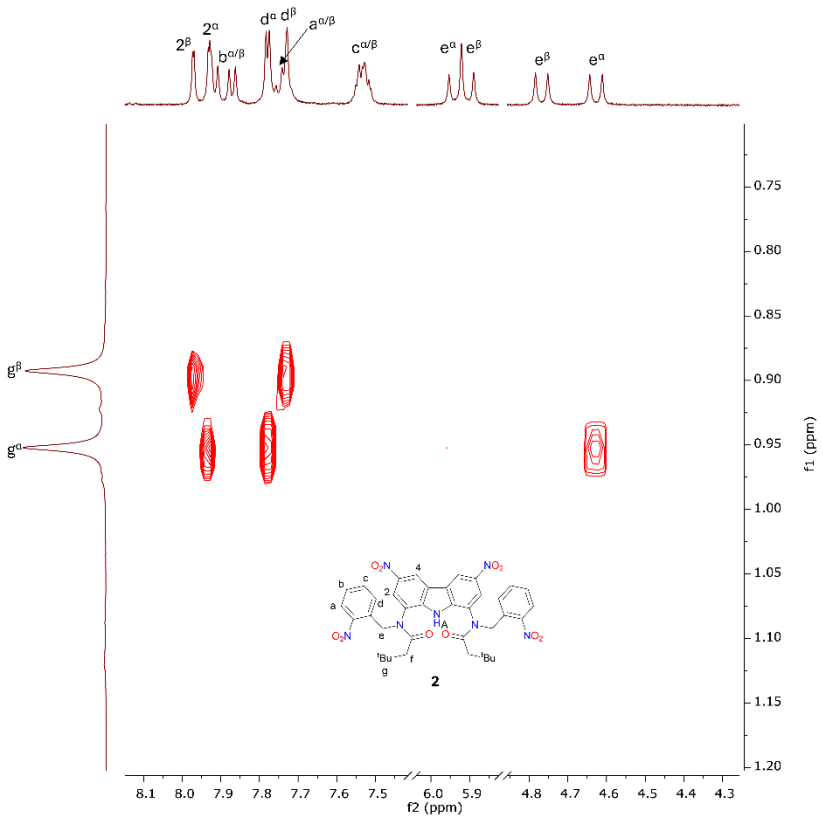

Figure S15. Section of 2D ^{1}H-^{1}H ROESY spectrum of **2** in DMSO-d_6.

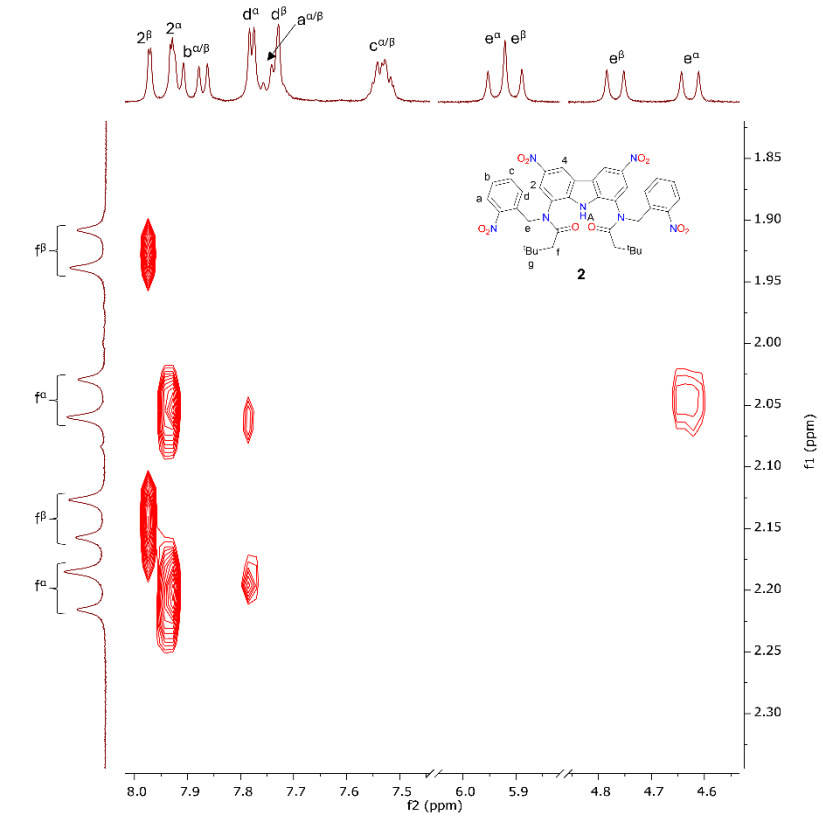

Figure S16. Section of 2D ^{1}H-^{1}H ROESY spectrum of **2** in DMSO-d_6.

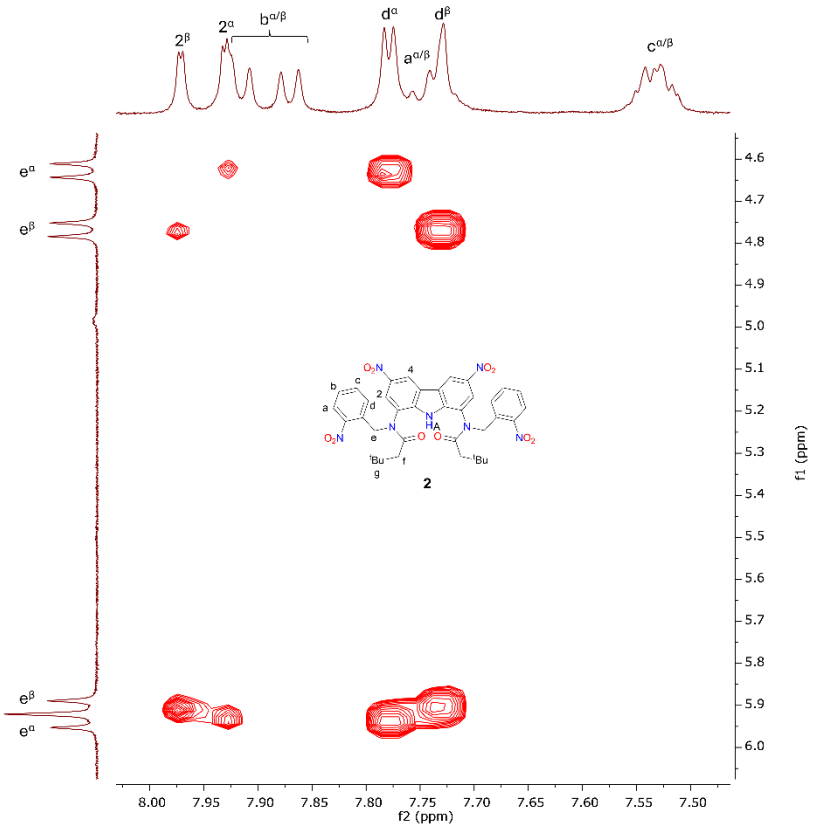

Figure S17. Section of 2D ^{1}H-^{1}H ROESY spectrum of **2** in DMSO-d_6.

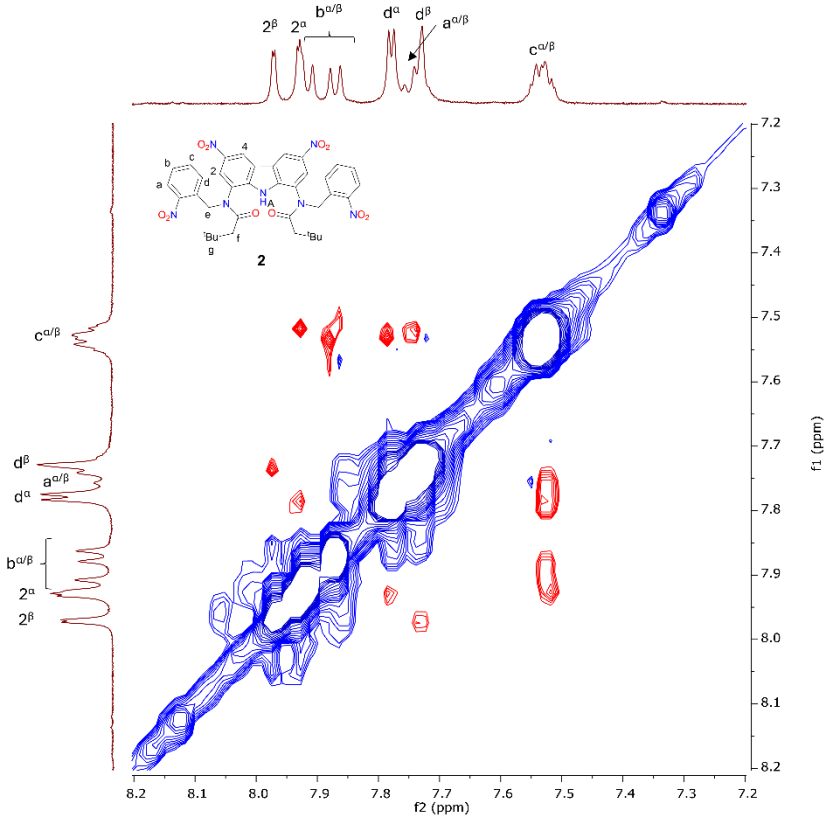

Figure S18. Section of 2D ^{1}H-^{1}H ROESY spectrum of **2** in DMSO-d_6.

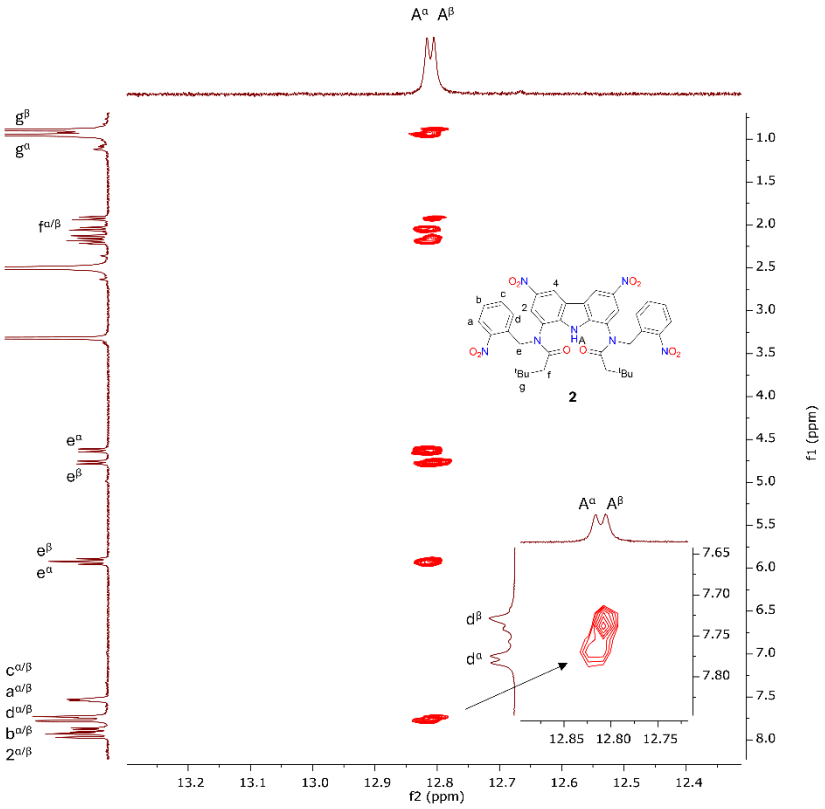

Figure S19. Section of 2D ^{1}H-^{1}H ROESY spectrum of **2** in DMSO-d_6.

3.2. Proton assignment in the ^{1}H NMR spectrum of 2

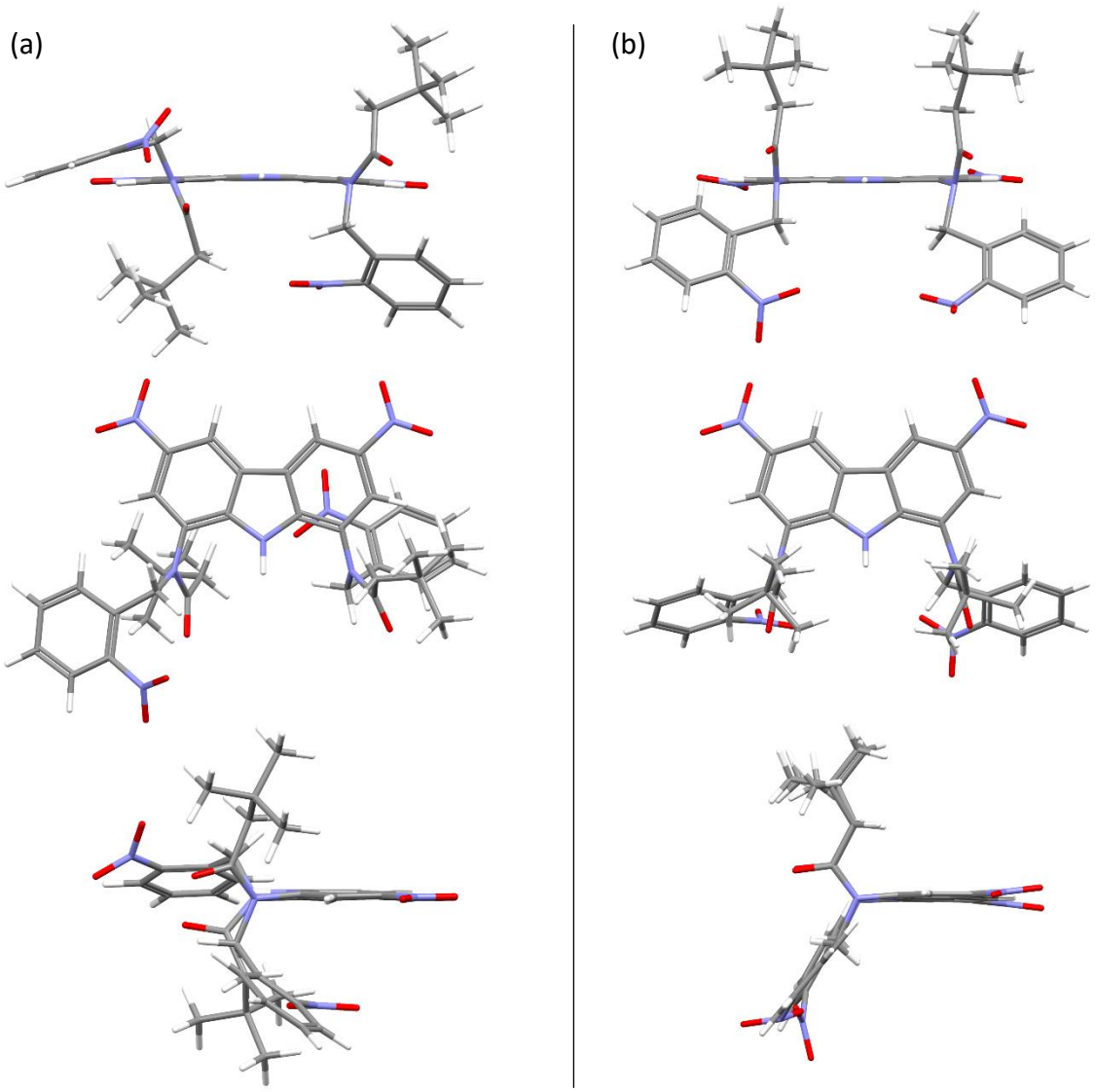

Figure S20. Structures of conformers: (a) **α** and (b) **β**.

The ^{1}H NMR spectrum of **2** consists of two sets of signals, which coalesce at 100-125°C (Figure S5). It suggests that the two sets originate from two distinct forms of **2**, which interconvert slowly on the NMR time scale (at room temperature). Based on the detailed analysis of 1D ^{1}H NMR and 2D ^{1}H-^{1}H COSY and ROESY spectra, the two sets of signals were attributed to two distinct conformations of **2**, denoted here as **α** and **β** (Fig. S20). The two conformations differ by the mutual disposition of the ONB groups: in **α**, the two ONB groups are placed on the opposite side of the carbazole plane, while in **β** the ONB groups are placed on the same side. The interconversion between the two conformations requires rotation of one of the amide arms around the $C_{carbazole}$-N_{amide} single bond. Apparently, this rotation is hindered by steric congestion caused by the two bulky groups (ONB and *t*-BuCH_2C=O) on the amide nitrogen atom.

As shown in Fig. S20, conformation **α** has a C_2 axis of symmetry, while conformation **β** has a plane of symmetry. Therefore, in both conformations the symmetrically equivalent protons from both sides of the central carbazole NH have the same chemical shift (in **α** they are homotopic, while in **β** they are enantiotopic). However, in each conformation the two CH_2 protons that are attached to the same

carbon atom are diastereotopic with respect to each other, and thus produce separate signals (doublets, due to the coupling with each other). Thus, the *t*-BuC**H₂** protons f^{α} and f^{β} give, in total, 4 such doublets (two from **α** and two from **β**), in the range 1.90-2.22 ppm. They can be easily grouped into two pairs (f^{α} and f^{β}) based on COSY cross-peaks (Figure S10). The same concerns the *o*-nitrobenzyl C**H₂** protons e^{α} and e^{β} (Figure S11). They were classified as either e^{α} or e^{β} based on ROESY cross-peaks with protons $f^{\alpha/\beta}$ and $g^{\alpha/\beta}$ (Figure S15 and Figure S16).

The *t*-Bu protons g give one singlet for each of the two conformations: one appears at 0.893, and the other at 0.952 ppm. The peaks were assigned to either the α or β family based on ROESY cross-peaks with the neighbouring methylene protons f^{α} and f^{β} (Figure S14).

In the aromatic region, i.e. between 7.529 and 9.568 ppm, there are four signals from the carbazole CH protons 2 and 4: 2^{α}, 2^{β}, 4^{α} and 4^{β} (Figure S12). Protons $2^{\alpha/\beta}$ were distinguished from $4^{\alpha/\beta}$ based on ROESY cross-peaks with the neighbouring *t*-Bu protons g^{α} and g^{β} (Figure S15) and the ONB protons d^{α} and d^{β} (at 7.779 and 7.732 ppm, respectively, Figure S18). Signals from protons 4^{α} and 4^{β} are not separated well enough to assign them specifically to the **α** or **β** conformation, so they were jointly labelled $4^{\alpha/\beta}$.

The two leftmost peaks on the spectrum, at 12.816 and 12.805 ppm, come from the carbazole NHs and were labelled A^{α} and A^{β} on the basis of ROESY cross-peaks with protons e^{α}, f^{α}, g^{α} and e^{β}, f^{β}, g^{β}, respectively (Figure S19).

At this stage of the analysis the only unassigned signals come from the four aromatic protons a, b, c and d of the *o*-nitrobenzyl ring. Some of these signals partially overlap with other signals and therefore could not be assigned to the specific conformation **α** or **β**.

First, signals at 7.732 and 7.779 ppm were assigned to protons d^{α} and d^{β}, based on the aforementioned ROESY cross-peaks with the carbazole CH protons 2^{α} and 2^{β} and with carbazole NH protons A^{α} and A^{β} (Figure S19; the ONB protons d may come closer to the carbazole protons CH-2 and NH than protons a, b and c). Second, the partially overlapping multiplet at 7.529 ppm was assigned to protons c, because it gives COSY and ROESY cross-peaks with protons d and with signals at 7.870 and 7.916 ppm, (Figure S12 and Figure S18) meaning that it comes from a proton that is close to d and at the same time to some other aromatic proton of the ONB moiety. Accordingly, signals at 7.870 ppm and 7.916 ppm were assigned to protons b. The last signal, at around 7.748 ppm, was therefore assigned to protons a by simple elimination.

The assignment of a particular structure from Figure S20 to the signals labelled as **α** and **β** was based on the following considerations. There are two ROESY cross-peaks between the signals from the **α** set that are not observed in the **β** set: (1) the *t*-Bu protons g^{α} couple with the *o*-nitrobenzyl protons e^{α} (Figure S15), and (2) the *t*-BuC**H**$_2$ protons f^{α} couple with the aromatic ONB protons d^{α} (Figure S16). Thus, apparently, the *t*-BuCH_2 and the ONB moieties are in closer proximity in the **α** conformation than in the **β** conformation, suggesting that in **α** the *t*-BuCH_2 and the ONB groups are on the same side of the carbazole plane.

4. *In silico* studies

The geometry of **2** was optimized *in silico* starting from two conformations, in which ONB moieties were either on the opposite sides of carbazole plane (conformation **α**) or on the same sides of carbazole plane (conformation **β**)**.** The geometry optimization and vibrational frequencies calculation were done by Gaussian 16 v. C.01 package using wB97XD functional and 6-31++ G(d,p) basis set. The program was used to calculate the *Sum of electronic and thermal free energies* (G) for optimized structures.

Table S1. The sum of electronic and thermal free energies (G) for optimized structures calculated using Gaussian 16 package.

Structure	Sum of electronic and thermal free energies (G)	
	in hartree	in kJ/mol
α	-2605.401048	-6840480.452
β	-2605.402971	-6840485.500

The difference in Gibbs free energies between conformations **α** and **β** was calculated according to the following equation:

$$\Delta G = G^{\alpha} - G^{\beta} = 5.048836499 \text{ kJ/mol} \approx 5 \text{ kJ/mol}$$

Table S2. Atomic coordinates of the optimized structure of **2** in conformation **α** shown in Figure S20a.

Atom number	Atom type	x	y	z
1	C	7.1155	8.5494	11.9212
2	C	6.2892	6.3811	10.8260
3	C	5.9136	5.7830	12.1883
4	H	5.1642	4.9956	12.0523
5	H	5.4999	6.5364	12.8646
6	H	6.7863	5.3436	12.6817
7	C	10.2476	10.4306	9.2755
8	C	11.6282	10.3237	9.4711
9	C	12.4450	10.5492	8.3753
10	H	13.5170	10.4257	8.4614
11	C	11.8845	10.9107	7.1465
12	C	10.5178	11.0141	6.9366
13	H	10.1348	11.2663	5.9556
14	C	9.6878	10.7602	8.0223
15	C	8.2488	10.6997	8.1948
16	C	7.1664	10.8969	7.3437
17	H	7.2842	11.1836	6.3061
18	C	6.8099	5.2703	9.9025
19	H	7.0930	5.6684	8.9221
20	H	6.0382	4.5079	9.7507
21	H	7.6902	4.7814	10.3323
22	C	5.9010	10.7081	7.8775

23	C	5.6769	10.3124	9.2013
24	H	4.6623	10.1394	9.5343
25	C	6.7449	10.1151	10.0581
26	C	8.0280	10.3371	9.5408
27	C	5.0506	7.0270	10.1896
28	H	5.2868	7.4607	9.2115
29	H	4.6357	7.8156	10.8271
30	H	4.2684	6.2752	10.0427
31	C	12.0550	8.4093	10.9279
32	H	12.4116	8.2182	11.9401
33	H	11.0161	8.0936	10.8562
34	C	7.4390	7.4207	10.9683
35	H	7.7016	7.7808	9.9705
36	H	8.3172	6.9154	11.3788
37	C	14.7469	6.6054	8.0494
38	H	15.4413	6.1928	7.3261
39	C	15.1989	7.0687	9.2824
40	H	16.2542	7.0204	9.5288
41	C	14.3024	7.6067	10.1996
42	H	14.6609	8.0031	11.1448
43	C	12.9330	7.6802	9.9313
44	C	12.5116	7.1991	8.6843
45	C	13.3956	6.6815	7.7423
46	H	13.0154	6.3465	6.7849
47	C	12.9411	10.6190	11.5600
48	C	12.9174	12.1254	11.3816
49	H	12.4230	12.5138	12.2808
50	H	12.2940	12.4053	10.5288
51	C	14.3013	12.8124	11.2437
52	C	14.0380	14.2941	10.9329
53	H	13.4862	14.4139	9.9936
54	H	14.9832	14.8384	10.8382
55	H	13.4576	14.7680	11.7324
56	C	15.1094	12.7107	12.5447
57	H	14.5529	13.1410	13.3847
58	H	16.0483	13.2660	12.4424
59	H	15.3398	11.6739	12.7950
60	C	15.0975	12.1919	10.0876
61	H	15.2731	11.1218	10.2492
62	H	16.0760	12.6746	9.9994
63	H	14.5814	12.3214	9.1304
64	C	6.1165	10.7202	12.3931
65	H	5.8150	11.6057	11.8301
66	H	6.9314	10.9994	13.0582
67	C	4.9205	10.1994	13.1719

68	C	3.7168	10.0243	12.4845
69	H	3.6631	10.3279	11.4436
70	C	2.5929	9.4722	13.0881
71	H	1.6756	9.3615	12.5195
72	C	2.6522	9.0609	14.4165
73	H	1.7857	8.6221	14.8987
74	C	3.8337	9.2177	15.1287
75	H	3.9162	8.9001	16.1610
76	C	4.9375	9.7943	14.5098
77	N	9.2393	10.1984	10.1775
78	H	9.3732	9.9545	11.1471
79	N	12.1352	9.8627	10.7152
80	N	11.0969	7.2323	8.2804
81	N	12.7908	11.1442	6.0188
82	N	4.7339	10.9046	7.0110
83	N	6.5817	9.7246	11.4125
84	N	6.1270	9.9656	15.3592
85	O	7.2545	8.4300	13.1309
86	O	10.2405	7.0031	9.1269
87	O	10.8518	7.4684	7.1082
88	O	13.5701	10.0741	12.4512
89	O	13.9917	11.0239	6.2203
90	O	12.2952	11.4471	4.9437
91	O	4.9353	11.2298	5.8505
92	O	3.6260	10.7332	7.5014
93	O	6.8001	10.9771	15.2058
94	O	6.3415	9.1132	16.2024

Table S3. Atomic coordinates of the optimized structure of **2** in conformation **β** shown in Figure S20b.

Atom number	Atom type	x	y	z
1	C	7.7940	10.0580	13.5220
2	C	7.3790	12.6050	13.7240
3	C	5.9490	12.4460	13.1910
4	H	5.3160	13.2650	13.5490
5	H	5.4960	11.5070	13.5300
6	H	5.9270	12.4620	12.0960
7	C	10.3530	9.6560	9.3740
8	C	11.7410	9.5900	9.2190
9	C	12.2560	9.8680	7.9630
10	H	13.3230	9.8290	7.7820
11	C	11.3930	10.2200	6.9190
12	C	10.0190	10.3330	7.0710
13	H	9.4010	10.6330	6.2330
14	C	9.4930	10.0530	8.3280

15	C	8.1580	10.0990	8.8960
16	C	6.9070	10.4580	8.4040
17	H	6.7450	10.7480	7.3730
18	C	7.9770	13.9200	13.2010
19	H	9.0050	14.0530	13.5570
20	H	7.3890	14.7740	13.5510
21	H	7.9890	13.9460	12.1050
22	C	5.8460	10.4420	9.2970
23	C	5.9810	10.0830	10.6420
24	H	5.1110	10.1100	11.2870
25	C	7.2160	9.6980	11.1350
26	C	8.2940	9.7110	10.2460
27	C	7.3650	12.6330	15.2580
28	H	8.3790	12.7450	15.6570
29	H	6.9460	11.7150	15.6750
30	H	6.7670	13.4820	15.6080
31	C	13.0890	7.8790	10.3740
32	H	13.2750	7.6270	11.4200
33	H	12.3120	7.2100	10.0050
34	C	8.2790	11.4570	13.1940
35	H	9.2650	11.5430	13.6630
36	H	8.4110	11.5890	12.1160
37	C	16.7470	7.4970	8.0450
38	H	17.6530	7.4170	7.4540
39	C	16.4230	8.6870	8.6930
40	H	17.0810	9.5460	8.6150
41	C	15.2530	8.7860	9.4370
42	H	15.0120	9.7240	9.9230
43	C	14.3740	7.7080	9.5780
44	C	14.7450	6.5200	8.9360
45	C	15.8980	6.4070	8.1630
46	H	16.1110	5.4660	7.6710
47	C	12.8570	10.1260	11.3560
48	C	12.2420	11.5140	11.2380
49	H	11.1600	11.4150	11.4030
50	H	12.3500	11.8500	10.2000
51	C	12.7870	12.6100	12.1750
52	C	12.0620	13.9120	11.7930
53	H	12.2680	14.1960	10.7550
54	H	12.3890	14.7340	12.4370
55	H	10.9760	13.8090	11.9080
56	C	12.4870	12.2920	13.6470
57	H	11.4080	12.1790	13.8070
58	H	12.8290	13.1140	14.2860
59	H	12.9830	11.3740	13.9660

60	C	14.2970	12.7940	11.9670
61	H	14.8490	11.9010	12.2710
62	H	14.6610	13.6380	12.5620
63	H	14.5240	13.0070	10.9150
64	C	7.0050	7.8570	12.7480
65	H	7.4000	7.6090	13.7330
66	H	7.4680	7.2110	12.0050
67	C	5.4960	7.7130	12.7590
68	C	4.8080	8.1460	13.8980
69	H	5.3910	8.4890	14.7480
70	C	3.4190	8.1660	13.9460
71	H	2.9170	8.5000	14.8480
72	C	2.6730	7.7690	12.8370
73	H	1.5900	7.7920	12.8640
74	C	3.3250	7.3520	11.6860
75	H	2.7750	7.0610	10.7990
76	C	4.7170	7.3120	11.6680
77	N	9.6130	9.4360	10.5110
78	H	9.9740	9.1100	11.3950
79	N	12.5640	9.2430	10.3270
80	N	13.9250	5.3080	9.0560
81	N	11.9810	10.5150	5.6070
82	N	4.5130	10.8210	8.8180
83	N	7.4000	9.2470	12.4720
84	N	5.3300	6.8650	10.4070
85	O	7.7890	9.6330	14.6690
86	O	13.2790	5.1560	10.0860
87	O	13.9480	4.5100	8.1320
88	O	13.5640	9.7660	12.2840
89	O	13.1960	10.4330	5.4970
90	O	11.2210	10.8280	4.7020
91	O	4.3970	11.1190	7.6390
92	O	3.5980	10.8220	9.6290
93	O	6.3350	6.1690	10.4620
94	O	4.7860	7.2090	9.3680

5. Photo-deprotection studies

5.1. General procedure of photo-deprotection studies

All the reagents were weighted separately on a Mettler Toledo Excellence XA105DU analytical balance (readability 0.01 mg) in screw-capped vials sealed with Teflon-covered septa. All the solvent/solution manipulations were done using gas-tight Hamilton glass syringes. UV-vis studies were performed in a septum-sealed screw-cap precision cell made of SUPRASIL Quartz (optical path length: 10 mm). NMR studies were performed in Standard Series Economy NMR tubes (HTPLUS, diameter: 5 mm) purchased from Euroisotop.

5.2. Photo-deprotection controlled by UV-vis

Samples of 5×10^{-5} M solution of **2** in MeOH were placed in quartz cuvettes (3 ml in each cuvette). Next, the samples were inserted into pre-equilibrated photoreactor (for details see Section 1.3) and irradiated for specified time (0 s – 120 s). Immediately after the irradiation UV-vis spectra of the samples were measured. The spectra of 5×10^{-5} M solution of **1** were measured both before and after irradiation, and turned out to be exactly same.

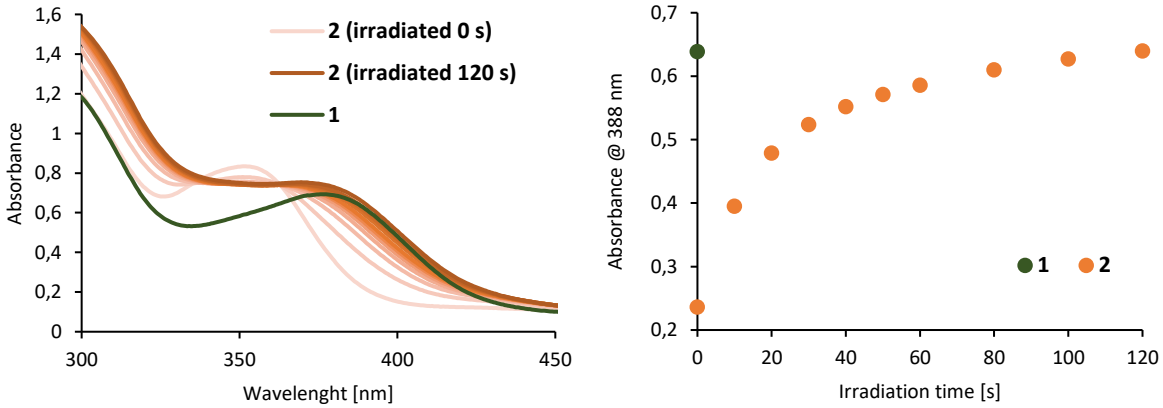

Figure S21. (left) UV-vis spectra of 5×10^{-5} M solutions of **2** measured after irradiation by 365 nm light for a specified time and UV-vis spectrum of 5×10^{-5} M solution of **1**. (right) Absorbance @ 388 nm of 5×10^{-5} M solution of **1**, and absorbance @ 388 nm of 5×10^{-5} M solutions of **2** plotted against irradiation times.

5.3. Photo-deprotection controlled by NMR

Four NMR tubes were filled with a solution of **2** in DMSO-d_6 (2 mM, 0.5 ml in each tube). The samples were inserted into pre-equilibrated photoreactor (for details see Section 1.3), and irradiated for specified time (0 s, 5 min, 30 min, 1 h). Immediately after the irradiation, the ^{1}H NMR spectra of the samples were acquired (Agilent 400 MHz).

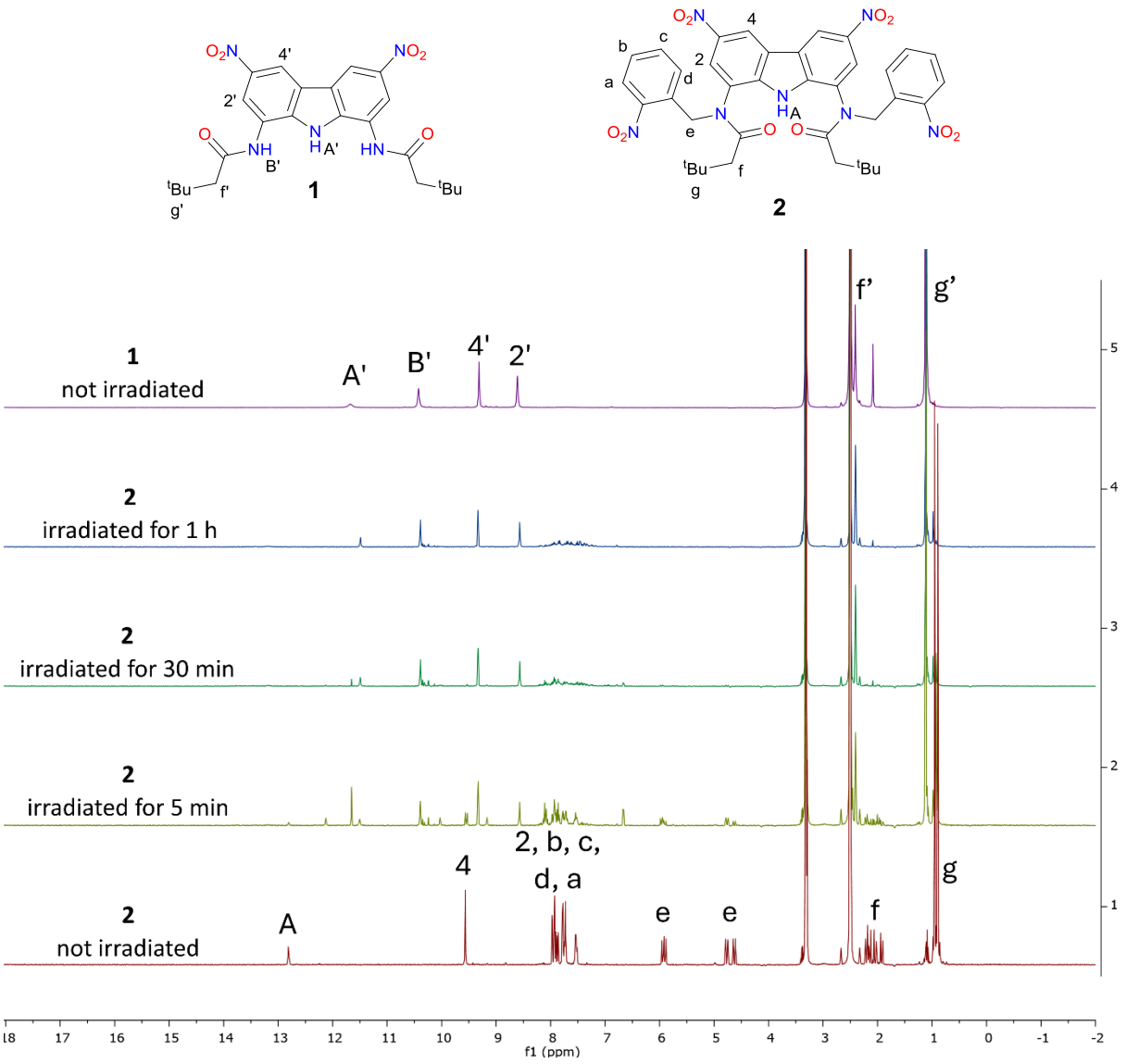

Figure S22. ^{1}H NMR spectra of 2 mM solutions of **2** in DMSO-d_6 obtained after irradiation by 365 nm light over specified time and ^{1}H NMR spectrum of 2 mM solution of **1** (top). The spectra were recorded using Agilent 400 MHz NMR instrument.

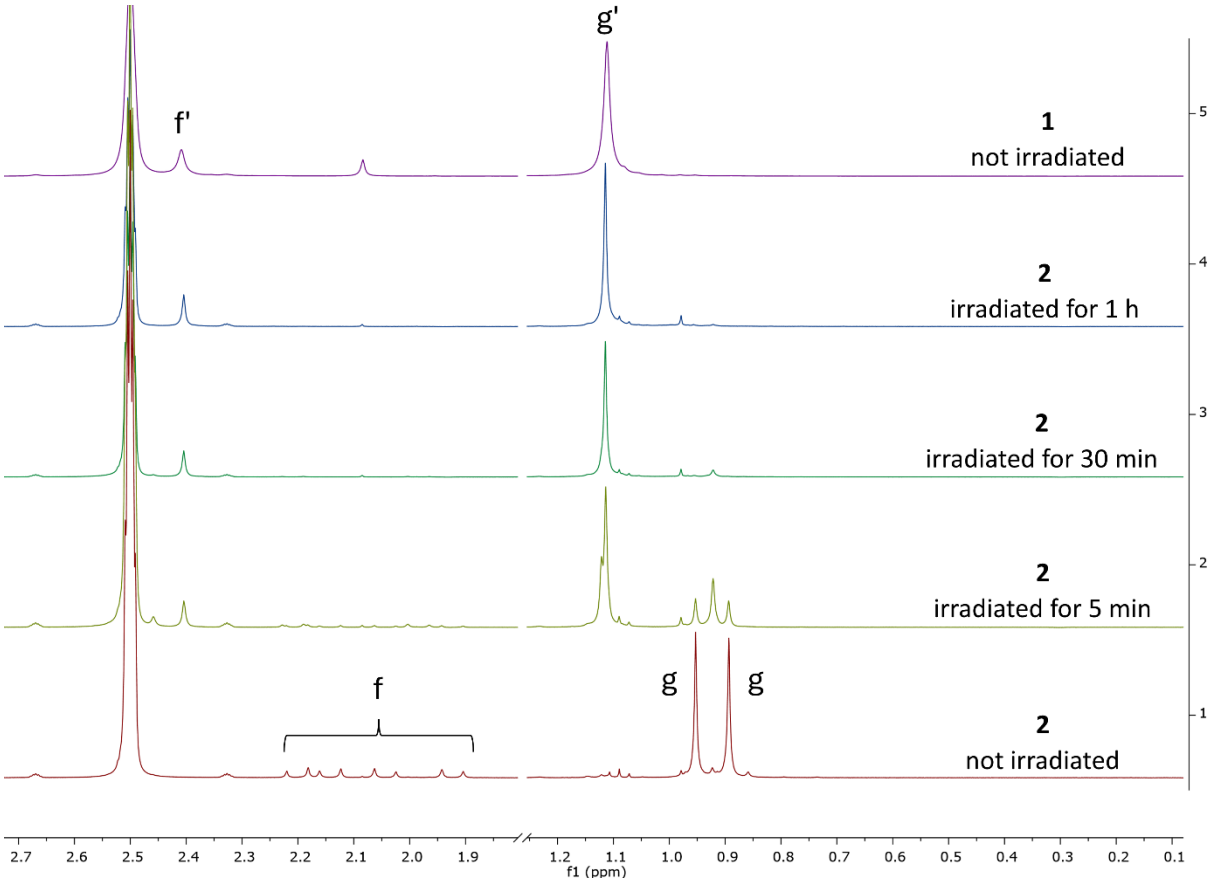

Figure S23. Section of the ^{1}H NMR spectra of 2 mM solutions of **2** in DMSO-d_6 obtained after irradiation by 365 nm light over specified time and ^{1}H NMR spectra of 2 mM solution **1** (top). Recorded using Agilent 400 MHz NMR instrument.

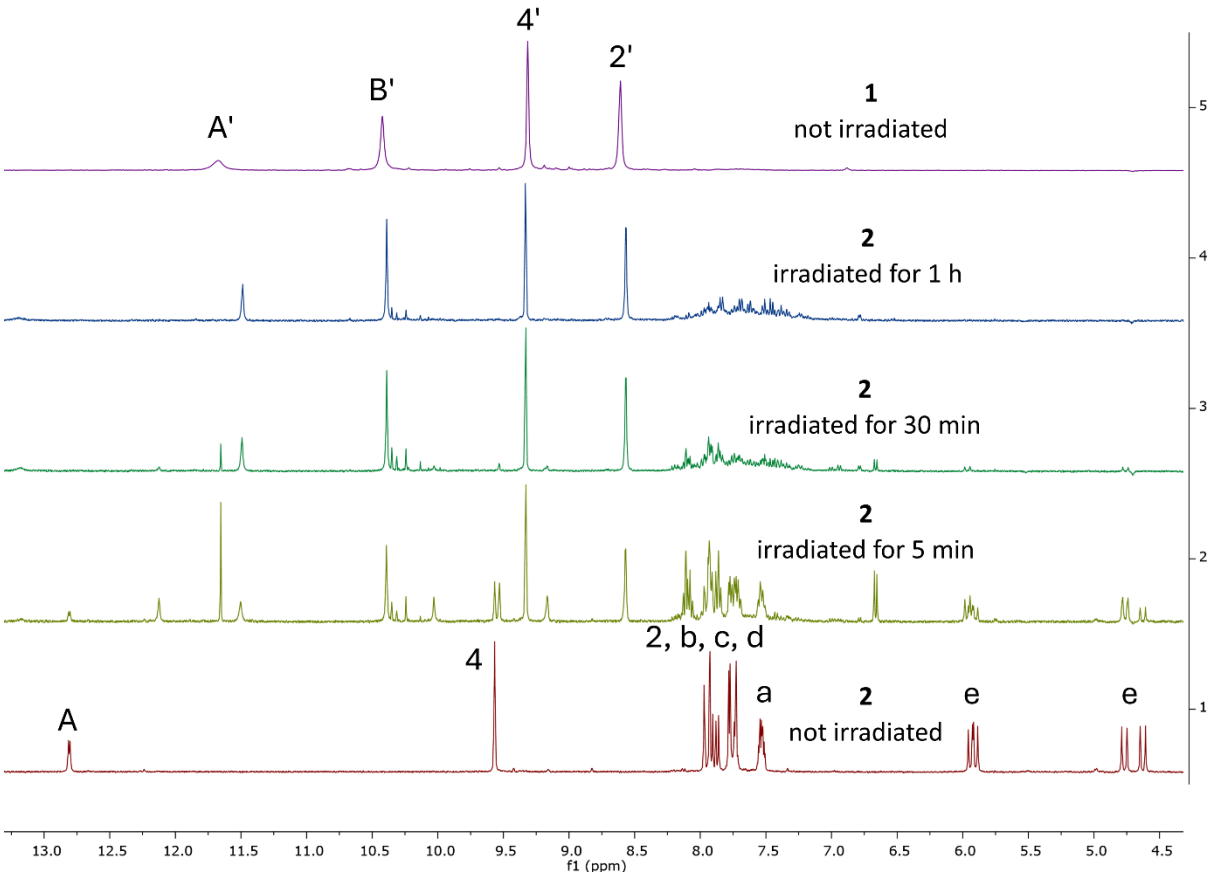

Figure S24. Section of ^{1}H NMR spectra of 2 mM solutions of **2** in DMSO-d_6 obtained during irradiation by 365 nm light over specified time and ^{1}H NMR spectra of 2 mM solution of **1** (top). Recorded using Agilent 400 MHz NMR instrument.

6. Transport studies

6.1. Photobleaching of lucigenin and SPQ

In a volumetric flask 25 ml of aqueous solution containing 225 mM $NaNO_3$ and 10^{-5} M lucigenin or SPQ was prepared. Next, 10 ml of the solution was transferred into a glass vial and pH was adjusted to either 5.4 or 7.4 by the addition of HNO_3 or NaOH respectively. 3 ml of the resulting solution was added into a 10×10 mm quartz cuvette. The cuvette was inserted into the pre-equilibrated photoreactor (for details see Section 1.3) and irradiated by 365 nm light for a specified time (0 s, 10 s, 20 s, 30 s, 90 s). After the irradiation, the fluorescence spectrum of each solution was measured (lucigenin: λ_{EX} = 455 nm; SPQ: λ_{EX} = 344 nm).

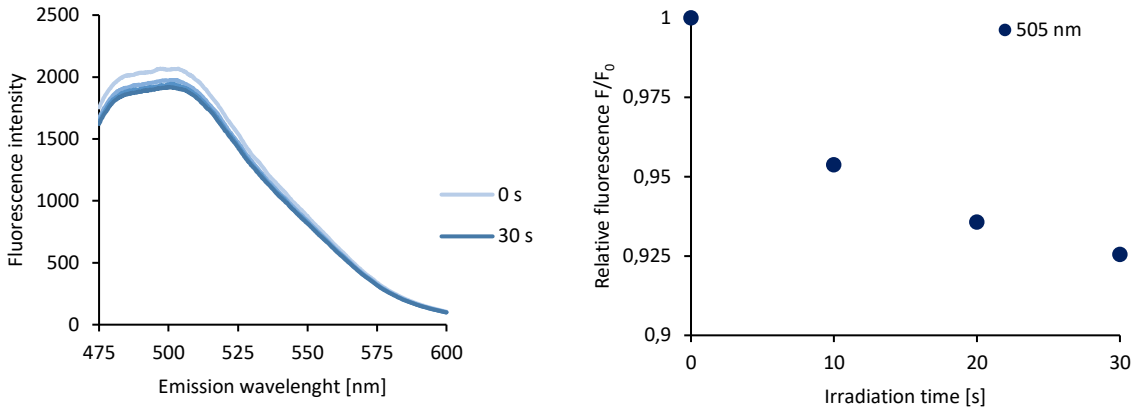

Figure S25. Left: fluorescence spectra of aqueous solutions of lucigenin (10^{-5} M) and $NaNO_3$ (225 mM) in pH 5.4, obtained after irradiation by 365 nm light. Right: relative fluorescence of the beforementioned solutions @ 505 nm.

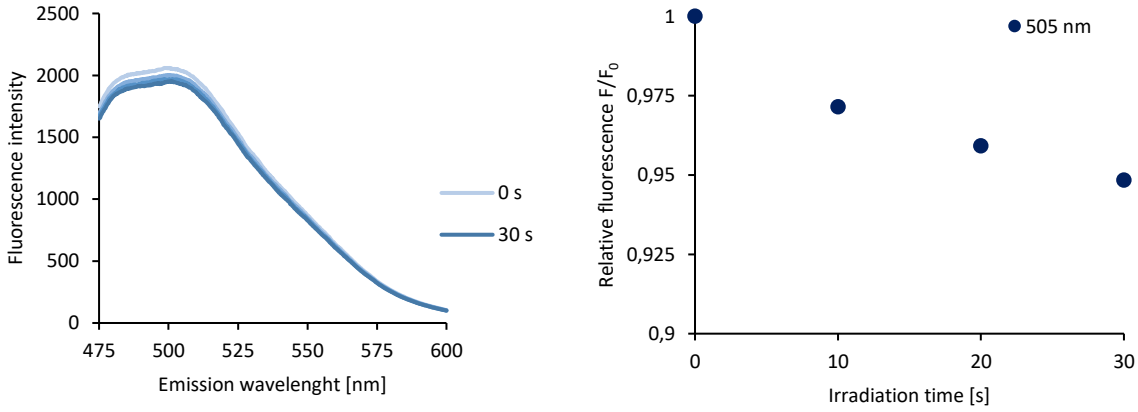

Figure S26. Left: fluorescence spectra of aqueous solutions of lucigenin (10^{-5} M) and $NaNO_3$ (225 mM) in pH 7.4 obtained after irradiation by 365 nm light. Right: relative fluorescence of the beforementioned solutions @ 505 nm .

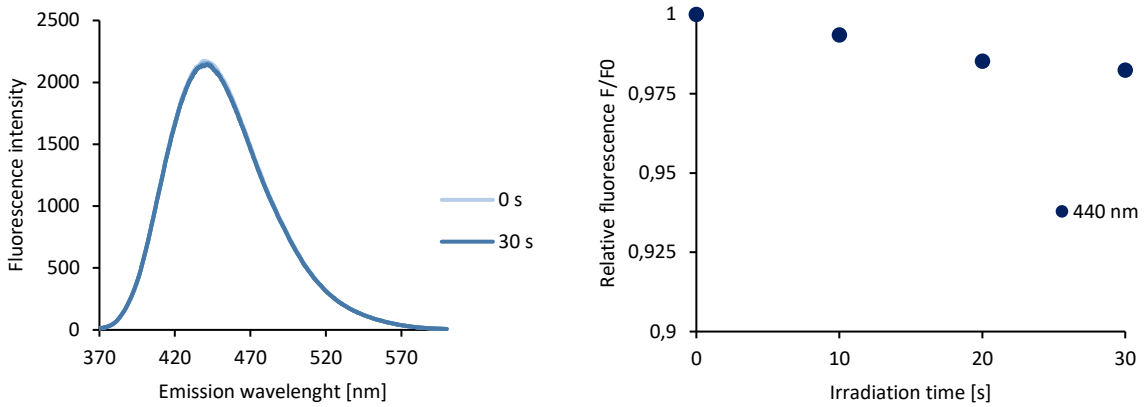

Figure S27. Left: fluorescence spectra of aqueous solutions of SPQ (10^{-5} M) and $NaNO_3$ (225 mM) in pH 5.4 obtained after irradiation by 365 nm light. Right: relative fluorescence of the beforementioned solutions @ 440 nm.

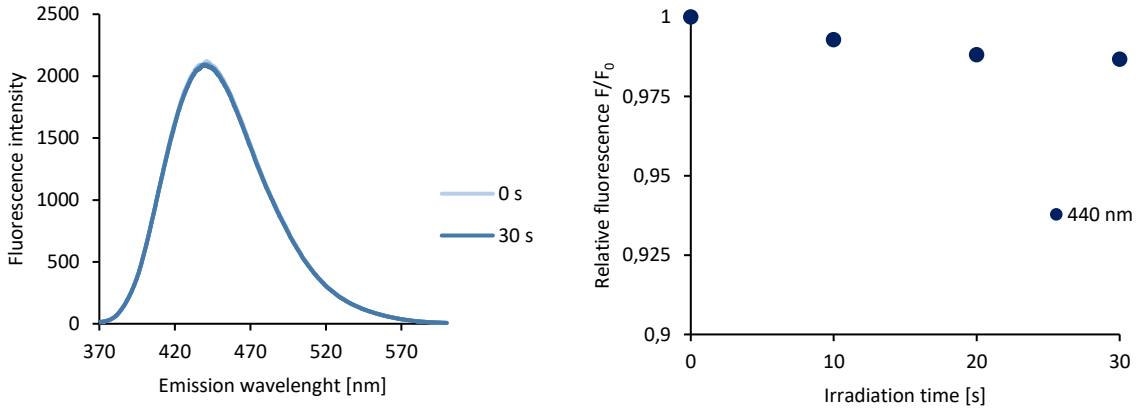

Figure S28. Left: fluorescence spectra of aqueous solutions of SPQ (10^{-5} M) and $NaNO_3$ (225 mM) in pH 7.4 obtained after irradiation by 365 nm light. Right: relative fluorescence of the beforementioned solutions @ 440 nm.

6.2. General procedure of transport studies

Our transport protocol published previously[3] was modified to accommodate pH control by phosphate buffer.

Preparation of Large Unilamellar Vesicles (LUVs)

Chloroform was freshly deacidified by passing through basic alumina. Next, 0.01 M chloroform solution of 1-palmitoyl-2-oleoyl-sn-glycero-3-phosphocholine (POPC, 420 µl, 4.2 µmol) and 0.01 M chloroform solution of cholesterol (180 µl, 1.8 µmol) was added into a 5 ml round-bottom flask, giving a POPC to cholesterol molar ratio 7:3. The solvent was evaporated on a rotary evaporator and dried under high vacuum for at least 1 hour. The lipid film was hydrated with 0.5 ml of aqueous solution containing SPQ (1 mM), $NaNO_3$ (225 mM) and phosphate buffer (20 mM, pH 5.4 or 7.4), sonicated for 30 seconds and vortexed for 1 hour. The suspension was subjected to 10 freeze-thaw cycles and diluted to 1 ml by the

addition of second portion (0.5 ml) of aqueous solution of SPQ (1 mM), $NaNO_3$ (225 mM) and phosphate buffer (20 mM, pH 5.4 or 7.4). Next, the mixture was extruded 29 times through a polycarbonate membrane (200 nm pore size). The unencapsulated SPQ was removed by passing the LUVs suspension through a column with Sephadex G-50 (*ca.* 2 g, superfine), eluting with aqueous solution of $NaNO_3$ (225 mM) and phosphate buffer (20 mM, pH 5.4 or 7.4) The collected fraction containing LUVs was diluted to 15 ml with 225 mM aqueous $NaNO_3$, yielding $c_{lipids} \approx 0.4$ mM.

Preparation of 1 M sodium chloride solution

A 5 ml volumetric flask was charged with sodium chloride (292 mg, 5 mmol) and topped to the line with aqueous solution of $NaNO_3$ (225 mM) and phosphate buffer (20 mM, pH 5.4 or 7.4).

Data acquisition

Into a quartz cuvette (10×10 mm) equipped with a small stirring bar, 3 ml of LUVs suspension was added ($c_{lipids} \approx 0.4$ mM, $n_{lipids} \approx 1.2\times10^{-6}$ mol), followed by DMSO solution of compound **1** or **2** (5 µl, 2.4×10^{-5} M, n = 1.2×10^{-10} mol, 0.01 mol% with respect to lipids) or DMSO alone (5 µl; blank). The cuvette was placed into a pre-equilibrated photoreactor (see Section 1.3 for details) and irradiated for a specified time (0 s, 10 s or 30 s) with UV light (365 nm). Next, the cuvette was inserted into a spectrofluorometer and its fluorescence was measured as a function of time (λ_{EX} = 344 nm, λ_{EM} = 440 nm). Immediately after insertion, transport was initiated by the addition of a pulse of NaCl (75 µl, 1 M) and fluorescence intensity was measured for 5 minutes. After this time, Triton-X (30 µl, 10% in water v/v) was added to lyse liposomes and the measurement was carried for additional 30 seconds. Finally, the pH of the resulting mixture was measured to check if it remained unchanged during the experiment.

6.3. The results of the transport studies

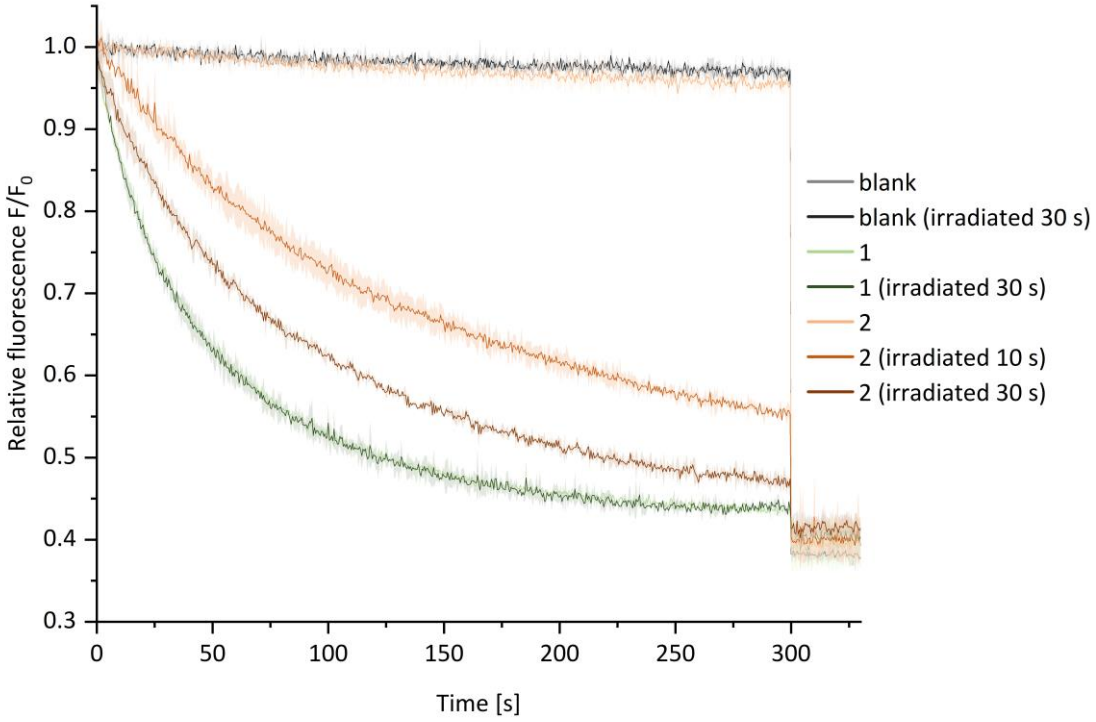

Figure S29. Transport of Cl^- mediated by compounds **1** or **2** post-incorporated into LUVs (as DMSO solutions) at 0.01 mol% (with respect to lipids), measured using SPQ assay in a solution containing 225 mM $NaNO_3$ and 20 mM phosphate buffer at pH 5.4. In the blank experiment, pure DMSO was added instead of the transporter solution. After *ca.* 5 min the liposomes were lysed by the addition of detergent. For irradiation, 365 nm light was used. The data were averaged from two separate experiments.

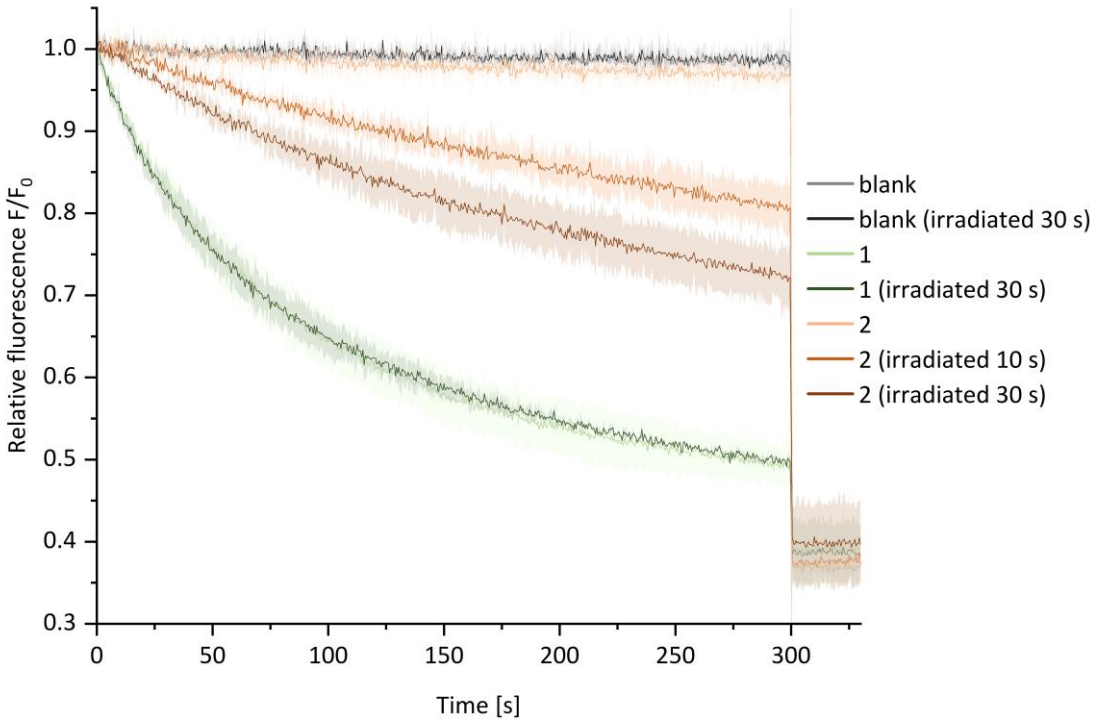

Figure S30. Transport of Cl^- mediated by compounds **1** or **2** post-incorporated into LUVs (as DMSO solutions) at 0.01 mol% (with respect to lipids), measured using SPQ assay in a solution containing 225 mM $NaNO_3$ and 20 mM phosphate buffer at pH 7.4. In the blank experiment, pure DMSO was added instead of the transporter solution. After *ca.* 5 min the liposomes were lysed by the addition of detergent. For irradiation, 365 nm light was used. The data were averaged from two separate experiments.

6.4. Quantification of the transport rates

As a first approximation, we can assume that the rate of anion transport (i.e., $d[A]/dt$, where $[A]$ is a concentration change inside the vesicles) is proportional to the difference between the extravesicular anion concentration $[A]_0$ and the intravesicular anion concentration $[A]$. Since the extravesicular anion concentration $[A]_0$ remains practically constant, the rate is proportional to the anion concentration inside the vesicle:

$$\frac{d[A]}{dt} = k([A]_0 - [A])$$

We can assume also that the free diffusion and carrier-mediated transport are independent of each other, so that:

$$\frac{d[A]}{dt} = k_{diffusion}([A]_0 - [A]) + k_{transport}([A]_0 - [A])$$

and

$$k = k_{diffusion} + k_{transport}$$

The solution of this equation is the exponential decay:

$$[A] = [A]_0(1 - e^{-kt})$$

In earlier work[4] we have plotted the decay of fluorescence F as the ratio F/F_0 (F_0 = initial fluorescence). Here we use F/F_0 for illustrative purposes but employ the reciprocal F_0/F for quantification. The use of F_0/F instead of F/F_0 was also justified in a previous publication.[5] According to the Stern–Volmer equation:

$$\frac{F_0}{F} = 1 + k_q\tau_0[Q]$$

(where k_q is the rate constant of the fluorescence quenching process and τ_0 is the lifetime of the emissive excited state of fluorophore in the absence of quencher Q) it is the F_0/F ratio which is proportional to the concentration of the quencher Q (in our case – to the concentration of chloride anions inside the vesicles, i.e., to $[A]$). Thus, plots of F_0/F are directly related to the increase of the anion concentration inside the vesicles, and the derivatives of these plots are proportional to the transport rates. The first 300 s of the traces were fitted therefore to a single exponential decay function:

$$\frac{F_0}{F} = y - a \cdot e^{-kx}$$

where *y*, *a* and k are fitting parameters.

The rate constants thus derived give approximate half-times, according to the following equation:

$$t_{1/2} = \frac{ln\,(2)}{k}$$

6.5. Transport rates

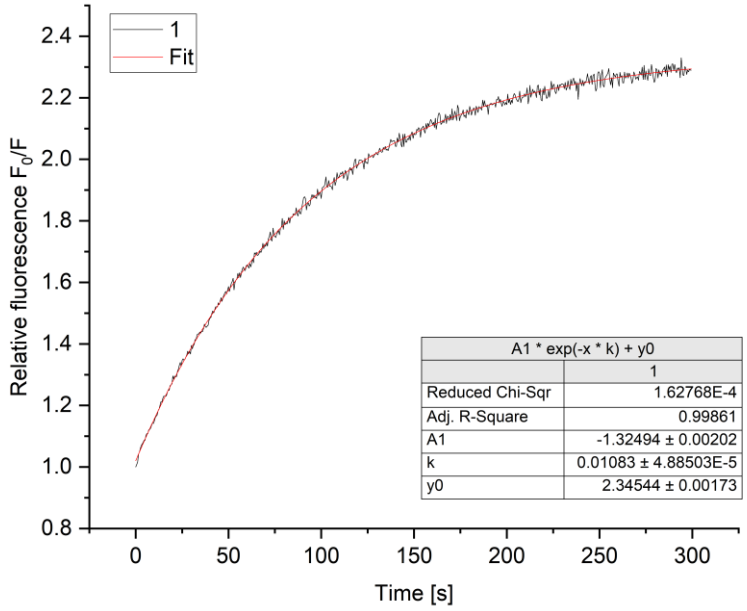

Figure S31. Averaged relative fluorescence intensity F_0/F and single exponential decay fits for the transport of Cl^- mediated by **1** post-incorporated into LUVs (as DMSO solutions) at 0.01 mol% (with respect to lipids), measured using SPQ assay, in a solution containing $NaNO_3$ (225 mM) and phosphate buffer (20 mM, pH 5.4).

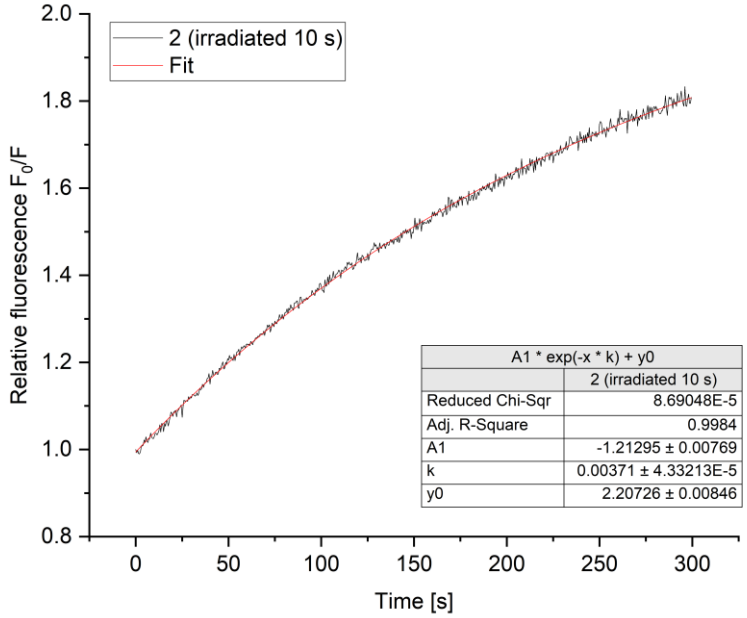

Figure S32. Averaged relative fluorescence intensity F_0/F and single exponential decay fits for the transport of Cl^- mediated by **2** post-incorporated into LUVs (as DMSO solutions) at 0.01 mol% (with respect to lipids), measured using SPQ assay, in a solution containing $NaNO_3$ (225 mM) and phosphate buffer (20 mM, pH 5.4). Prior to the addition of Cl^-, the LUVs suspension was irradiated by 365 nm light for 10 s.

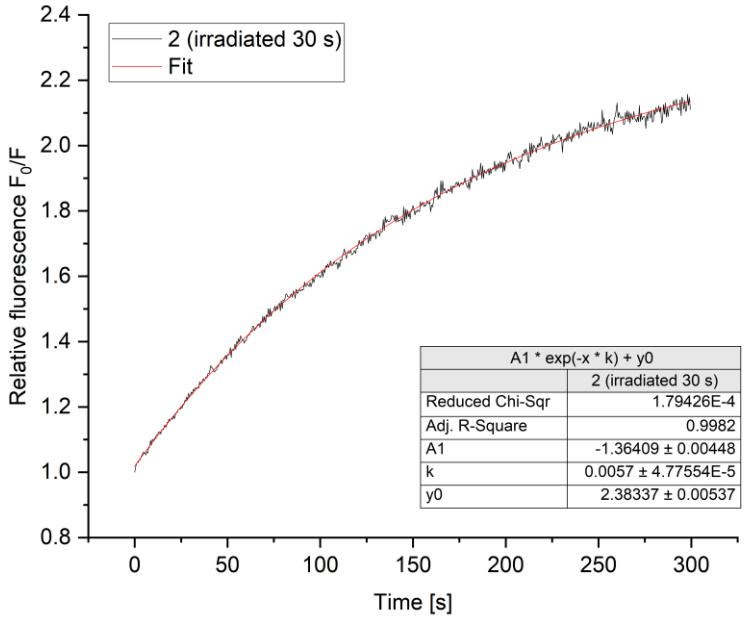

Figure S33. Averaged relative fluorescence intensity F_0/F and single exponential decay fits for the transport of Cl^- mediated by **2** post-incorporated into LUVs (as DMSO solutions) at 0.01 mol% (with respect to lipids), measured using SPQ assay, in a solution containing $NaNO_3$ (225 mM) and phosphate buffer (20 mM, pH 5.4). Prior to the addition of Cl^-, the LUVs suspension was irradiated by 365 nm light for 30 s.

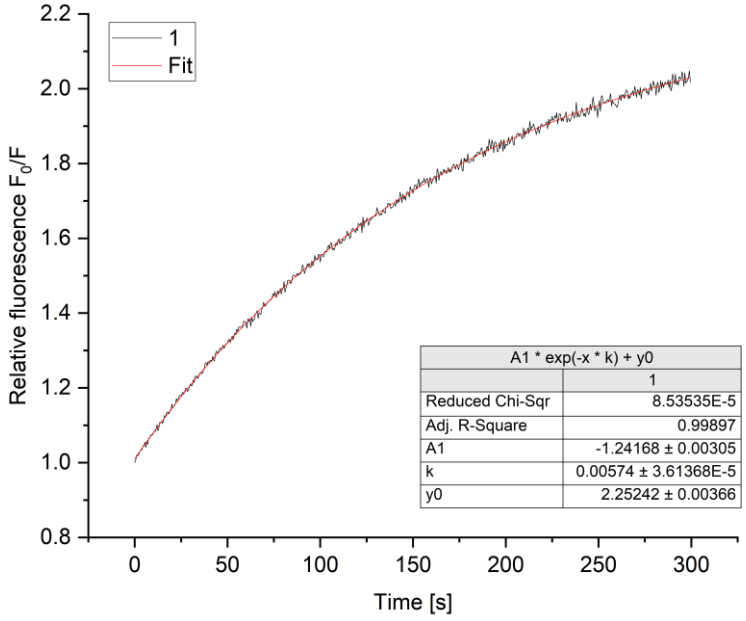

Figure S34. Averaged relative fluorescence intensity F_0/F and single exponential decay fits for the transport of Cl^- mediated by **1** post-incorporated into LUVs (as DMSO solutions) at 0.01 mol% (with respect to lipids), measured using SPQ assay, in a solution containing $NaNO_3$ (225 mM) and phosphate buffer (20 mM, pH 7.4).

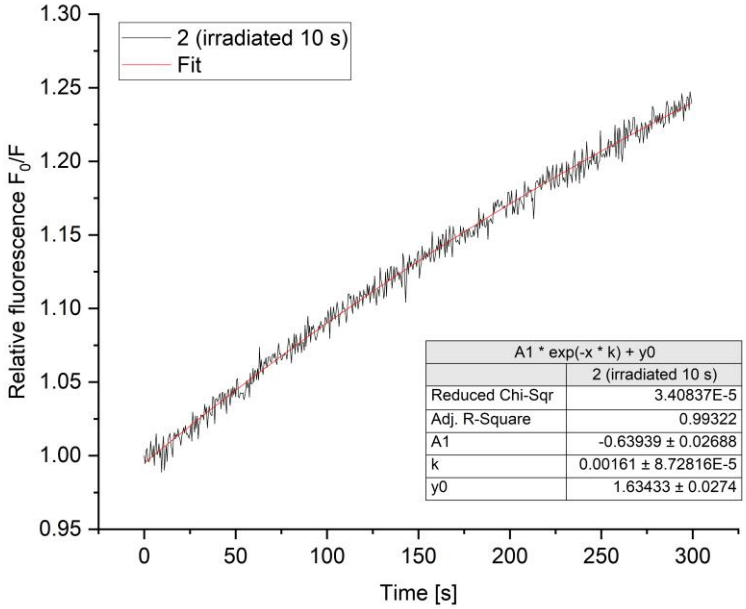

Figure S35. Averaged relative fluorescence intensity F_0/F and single exponential decay fits for the transport of Cl^- mediated by **2** post-incorporated into LUVs (as DMSO solutions) at 0.01 mol% (with respect to lipids), measured using SPQ assay, in a solution containing $NaNO_3$ (225 mM) and phosphate buffer (20 mM, pH 7.4). Prior to the addition of Cl^-, the LUVs suspension was irradiated by 365 nm light for 10 s.

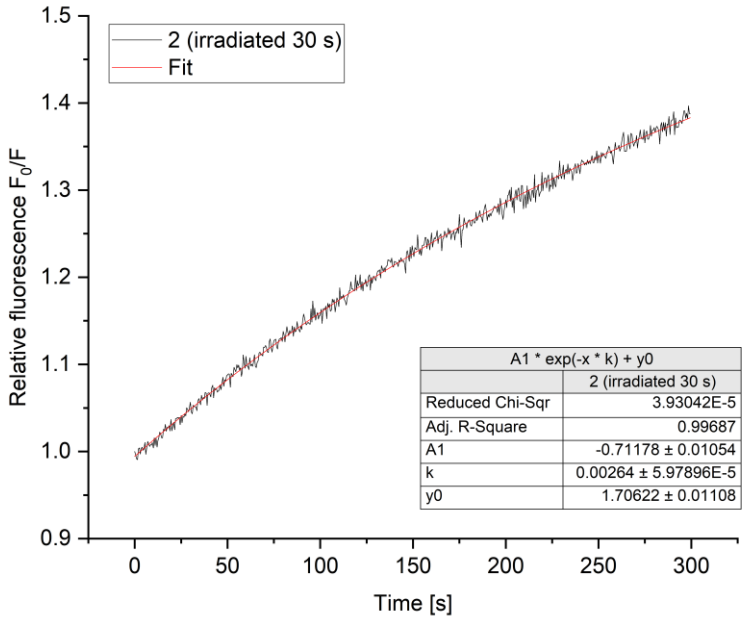

Figure S36. Averaged relative fluorescence intensity F_0/F and single exponential decay fits for the transport of Cl^- mediated by **2** post-incorporated into LUVs (as DMSO solutions) at 0.01 mol% (with respect to lipids), measured using SPQ assay, in a solution containing $NaNO_3$ (225 mM) and phosphate buffer (20 mM, pH 7.4). Prior to the addition of Cl^-, the LUVs suspension was irradiated by 365 nm light for 30 s.

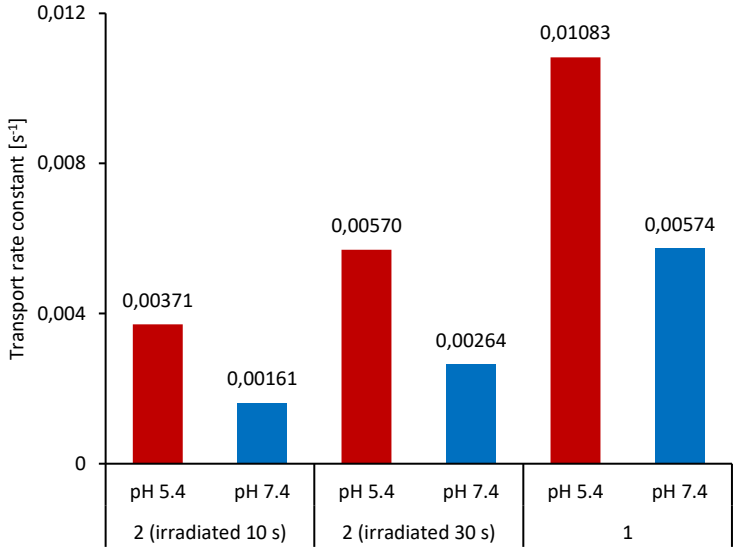

Figure S37. Rate constants of Cl^- transport mediated by compounds **1** or **2** post-incorporated into LUVs (as DMSO solutions) at 0.01 mol% (with respect to lipids), studied with SPQ assay in a solution containing 225 mM $NaNO_3$ and 20 mM phosphate buffer, pH 5.4 or 7.4. For irradiation, 365 nm light was used. Transport rates were calculated using Origin 2023 by fitting single exponential decay function to F_0/F traces (as described in Section 6.4).

7. References

1 Z. Kokan and M. J. Chmielewski, *J. Am. Chem. Soc.*, 2018, **140**, 16010.

2 K. Maslowska-Jarzyna, M. L. Korczak, J. A. Wagner and M. J. Chmielewski, *Molecules*, 2021, **26**, 3205.

3 K. Maslowska-Jarzyna, K. M. Bąk, B. Zawada and M. J. Chmielewski, *Chem. Sci.*, 2022, **13**, 12374.

4 R. Pomorski, M. García-Valverde, R. Quesada and M. J. Chmielewski, *RSC Adv.*, 2021, **11**, 12249.

5 X. Wu, N. Busschaert, N. J. Wells, Y.-B. Jiang and P. A. Gale, *J. Am. Chem. Soc.*, 2015, **137**, 1476.